https://doi.org/10.5194/acp-2020-655
Preprint. Discussion started: 1 September 2020

Atmospheric Chemistry and Physics Discussions

Cloud-scale modelling of the impact of deep convection on the fate of oceanic bromoform in the troposphere: a case study over the west coast of Borneo

Paul. D. Hamer[1,2], Virginie Marécal[2], Ryan Hossaini[3], Michel Pirre[4,*], Gisèle Krysztofiak[4], Franziska Ziska[5], Andreas Engel[6], Stephan Sala[6], Timo Keber[6], Harald Bönisch[6], Elliot Atlas[7], Kirsten Krüger[8], Martyn Chipperfield[9], Valery Catoire[4], Azizan A. Samah[10,11], Marecel Dorf[12], Phang Siew Moi[11], Hans Schlager[13], Klaus Pfeilsticker[14]

[1]Norwegian Institute for Air Research (NILU), Kjeller, Norway
[2]Centre National de Recherches Météorologiques, Université de Toulouse, Météo-France, CNRS, Toulouse, France
[3]Lancaster Environment Centre, Lancaster University, Lancaster, LA1 4YQ, UK
[4]Laboratoire de Physique et Chimie de l'Environnement et de l'Espace, CNRS and University of Orléans, UMR7328, Orléans, France
[5]GEOMAR Helmholtz Centre for Ocean Research Kiel, Kiel, Germany
[6]Institute for Atmospheric and Environmental Sciences, University of Frankfurt, Altenhöferallee 1, 60438 Frankfurt, Germany
[7]University of Miami, 4600 Rickenbacker Causeway, Miami, FL 33149
[8]Department of Geosciences, University of Oslo, Postboks 1022, Blindern, 0315 OSLO
[9]The Institute for Climate & Atmospheric, Science, School of Earth and Environment, University of Leeds, Leeds, UK
[10]National Antarctic Research Centre, University of Malaya, Kuala Lumpur 50603, Malaysia
[11]Institute of Ocean & Earth Sciences, University of Malaya, 50603 Kuala Lumpur, Malaysia
[12]Max Planck Institute for Chemistry, Department of Atmospheric Chemistry, Mainz, Germany
[13]Deutsches Zentrum für Luft- und Raumfahrt (DLR), Institut für Physik der Atmosphäre, Atmosphärische Spurenstoffe, Münchner Straße 20, 82234 Oberpfaffenhofen-Wessling, Germany
[14]Institute of Environmental Physics, Ruprecht-Karls-Universität Heidelberg, Im Neuenheimer Feld 229, D-69120 Heidelberg, Germany
[*]Retired

Correspondence to: Paul D. Hamer (paul.hamer@nilu.no)

Abstract. Coastal oceans emit bromoform ($CHBr_3$) that can be transported rapidly to the upper troposphere by deep convection. In the troposphere, the spatial and vertical distribution of $CHBr_3$ and its product gases (PGs) depend on emissions, chemical processing, transport by large scale flow, convection, and associated washout. This paper presents a modelling study on the fate of $CHBr_3$ and its PGs in the troposphere. A case study at cloud scale was conducted along the west coast of Borneo, when several deep convective systems triggered in the afternoon and early evening of November 19th 2011. These systems were sampled by the Falcon aircraft during the field campaign of the SHIVA project. We analyse these systems using a simulation with the cloud-resolving meteorological model C-CATT-BRAMS at 2 × 2 km resolution that describes transport, photochemistry, and washout of $CHBr_3$. We find that simulated $CHBr_3$ mixing ratios and the observed values in the boundary layer and the outflow of the convective systems agree. However, the model underestimates the background $CHBr_3$ mixing ratios in the upper troposphere, which suggests a missing source. An analysis of the simulated chemical speciation of bromine within and around each simulated convective system during the mature convective stage reveals that >85% of the bromine

https://doi.org/10.5194/acp-2020-655
Preprint. Discussion started: 1 September 2020


Atmospheric Chemistry and Physics Discussions

derived from $CHBr_3$ and its PGs is transported vertically to the point of convective detrainment in the form of $CHBr_3$ and that the remaining small fraction is in the form of organic PGs, principally insoluble brominated carbonyls produced from the photo-oxidation of $CHBr_3$. The model simulates that within the boundary layer and free troposphere, the inorganic PGs are only present in soluble forms, i.e., HBr, HOBr, and $BrONO_2$, and consequently, within the convective clouds, the inorganic PGs are almost entirely removed by wet scavenging. For the conditions of the simulated case study Br_2 plays no significant role in the vertical transport of bromine. This likely results from the small simulated quantities of inorganic bromine involved, the presence of HBr in large excess compared to HOBr and the less soluble BrO, and the relatively quick removal of soluble compounds within the convective column. This prevalence of HBr is a result of the wider simulated regional atmospheric composition whereby background tropospheric ozone levels are exceptionally low.

1 Introduction

Organic brominated compounds cause stratospheric ozone loss (Engel and Rigby, 2018). A compilation of model and observational evidence, shows that both longer lived (e.g., methyl bromide (CH_3Br)) organic bromine compounds and so-called very short-lived species (VSLS) are required to explain the ranges of total Br_y within the stratosphere (strat-Br_y) of 5±2 pptv (Engel and Rigby, 2018). Recent observation campaigns (Andrews et al., 2016; Navarro et al., 2015; Wales et al., 2018) show some minor variations but broadly agree with this compiled range.

Recent studies using global chemistry transport models (CTM) and chemistry climate models (CCMs) estimate the VSLS contribution to strat-Br_y to range from 2 - 8 pptv (Liang et al., 2010; Hossaini et al., 2012; Hossaini et al., 2016; Aschmann and Sinnhuber, 2013; Liang et al., 2014, Wales et al. 2018; Tegtmeier et al., 2020) which is broadly consistent with the ranges compiled in Carpenter et al. (2014) and Engel and Rigby (2018). The model estimates differ due to the considered VSLS and which assumptions are made for surface emissions, chemistry, and washout in the troposphere.

Brominated VSLS are primarily of biogenic and oceanic origin produced by macroalgae (Leedham et al., 2012) and phytoplankton. Observations indicate that VSLS emissions are larger towards coasts compared to the open ocean (e.g., Quack and Wallace, 2003, Carpenter et al., 2009). $CHBr_3$, with 3 Br atoms per molecule, has the largest emissions among the different brominated VSLS. For these reasons we focus on $CHBr_3$ in the present study.

Global estimates of $CHBr_3$ emissions range between 120 and 820 Gg/yr (Liang et al., 2010; Warwick et al., 2006; Butler et al. 2007, Ordoñez et al., 2012; Pyle et al., 2011; Ziska et al., 2013, Engel and Rigby, 2018). Most current inventories show that emissions are predominantly distributed in the tropics, but there is considerable uncertainty regarding the precise spatial and temporal distribution of emissions at the regional (Ashfold et al., 2014 Fiehn et al 2017, 2018) and the global scale (Hossaini et al. 2013). Furthermore, recent work suggests that the extratropical zones may also be important source regions (Keber et al., 2020).

Tropical deep convection is the primary mechanism by which emissions of short-lived tropospheric trace gases and aerosols are transported to the upper troposphere. If convective outflow detrains above the level of zero radiative heating (LZRH), it

https://doi.org/10.5194/acp-2020-655
Preprint. Discussion started: 1 September 2020


Atmospheric Chemistry and Physics Discussions

undergoes net radiative heating and eventual buoyancy-driven slow ascent to the stratosphere. For clear sky conditions, the LZRH is approximately 15 km in the tropics, and can be as low as 11 km for air masses within clouds resulting from convective outflow (Corti et al., 2005, 2006). Tropical deep convection can also loft air masses directly into the stratosphere through a process called convective over-shooting, but this process is less frequent (e.g. Liu and Zipser 2005, Luo et al. 2008).

After emission, $CHBr_3$ undergoes oxidation in the troposphere during transport either via reaction with the hydroxyl radical (OH) or via photolysis (approximate lifetime of 16 days, Burkholder et al., 2018). The oxidation products are organic and inorganic product gases (PGs) (Hossaini et al., 2010; Krysztofiak et al., 2012). The most important organic PGs are the brominated organic peroxides, CBr_3O_2H, $CHBr_2O_2H$; and the brominated carbonyl species, CBr_2O and CHBrO. The inorganic PGs consist of the bromine radical (Br), molecular bromine (Br_2), bromine oxide (BrO), hypobromous acid (HOBr), hydrogen bromine (HBr), and bromine nitrate ($BrONO_2$). These PGs have a range of solubilities, and thus washout within convective systems is expected to exert a strong control on the vertical transport of bromine to the upper troposphere (Hossaini et al., 2010).

$CHBr_3$ is important at the global scale, but deep convection occurs at the local scale. Convective transport and the associated chemistry and washout of all bromine containing species (Br_y) cannot be simulated in detail with global 3-dimensional models because of their coarse resolution, and because of the complexity of the chemical processes (e.g. Hossaini et al., 2010). In global models, deep convection is a sub-grid scale process taken into account by parameterizations. These parameterizations are a known source of uncertainty for tracer transport, including $CHBr_3$, from the boundary layer to the upper troposphere (e.g. Hoyle et al. 2011, Liang et al., 2014; Hossaini et al., 2016; Butler et al., 2018). Regarding chemical processes and their interactions with liquid and ice hydrometeors, global models have made progress (Hossaini et al. 2012, Aschmann and Sinnhuber, 2013, Liang et al. 2014), but they still need to compromise between complexity and computing resources. The analysis of the detailed transport and chemical processes occurring within deep convection and in its vicinity needs fine scale modelling at the kilometre-resolution with detailed chemistry (e.g., Barth et al., 2001; Marécal et al., 2006). This knowledge, gained from studies at the convective scale, may then improve the representation of the fate of chemical species in global models.

Only two detailed model studies examining VSLS degradation chemistry (both gas and aqueous phase), which were idealised cases, have been carried out at the convective scale (Krysztofiak et al., 2012; Marécal et al., 2012). Krysztofiak et al. (2012) focused on developing and optimising a photochemical mechanism for $CHBr_3$ degradation for use within models, and they estimated Henry's Law coefficients for some of the organic bromine species within the optimised mechanism. Marécal et al. (2012) implemented the $CHBr_3$ photochemical scheme of Hossaini et al. (2010) in addition to aqueous phase uptake and chemistry based on the Henry's Law coefficients from Krysztofiak et al. (2012). Using idealised simulations of a tropical convective cloud, Marécal et al. (2012) explored the $CHBr_3$ chemistry at the cloud scale and highlighted the importance of aqueous phase processes for understanding source gas and PG chemistry and transport.

Given the limitations of the previous studies at the convective scale, we wish to expand upon that previous work, e.g., Marécal et al. (2012), by carrying out a real-world case study. In this paper we present a study based on a high-resolution cloud resolving

https://doi.org/10.5194/acp-2020-655
Preprint. Discussion started: 1 September 2020


Atmospheric Chemistry and Physics Discussions

modelling of the transport, chemistry, and washout of $CHBr_3$ and its derivatives within convective clouds along the west coast of Borneo. Specifically, we aim to look at the bromine compound speciation in the areas of convective entrainment and detrainment and both within and outside of several convective systems. The modelling is supported using aircraft observations of $CHBr_3$, which we use to establish the credibility of the simulated chemical processes.

Section 2 gives a description of the measurement campaign over the west coast of Borneo, it provides an overview of the case study, and it includes a description of the meteorological situation based on observations. Section 3 describes the model used, its new developments and the simulation setup. Section 4 presents our modelling results, which includes: i) an evaluation of the simulated meteorology with respect to the situation described in Sect. 2; ii) a detailed analysis of the transport, chemistry and washout of bromoform and its PGs; and iii) a discussion of the chemistry. Section 5 discusses the limitations, Sect. 6 presents a summary and our conclusions, and Sect. 7 presents a brief outlook.

2 The SHIVA Campaign and Case Study Overview

The EU funded SHIVA ('Stratospheric Ozone: Halogen Impacts in a Varying Atmosphere') project (http://shiva.iup.uni-heidelberg.de/) was designed to address uncertainties in our understanding of VSLS, their contribution to stratospheric bromine, and their impact on stratospheric ozone. A measurement campaign within SHIVA was carried out in November 2011 that focused on the South East Asia Maritime Continent (SEA-MC) to better understand the emissions and the transport of oceanic VSLS, including $CHBr_3$, to the upper troposphere and stratosphere. This region was selected for two reasons. First, it represents globally the most important region for deep convection (Liu and Zipser, 2005) and second, the SEA-MC was believed to be an important region for VSLS emissions due to its many coastlines and its location in the tropics. The campaign primarily relied on measurements of chemical species onboard the Deutsches Zentrum für Luft- und Raumfahrt (DLR) Falcon aircraft based in Miri, Sarawak, Malaysia, which were complemented by ship and ground-based observations (Pfeilsticker et al., 2013).

We selected a case study from the SHIVA campaign on the afternoon of 19 November 2011. Figure 1 shows hourly maps of brightness temperature contours measured by the 11 μm channel IR108 on board the MTSAT-2 satellite. Note that the brightness temperatures contours in Fig. 1 are chosen to highlight only cloud tops in the upper troposphere. The brightness temperature imagery illustrates that several deep convective systems initiated inland along the West coast of Borneo where $CHBr_3$ emissions are expected to be strong (Ziska et al., 2013). The Falcon aircraft sampled two of these convective systems, which we henceforth refer to as Obs_Conv1 and Obs_Conv2 and are shown in the blue box and pink box in Fig. 1, respectively. The temporal evolution of both convective systems develops over several hours (05 UTC to 12 UTC) and is shown in Figs 1 (a) through (h), which indicates that the two follow a similar development scenario. They were both initiated early afternoon inland close to the west coast of Borneo from offshore low-level winds encountering the steep topography of the island. These low levels winds come from the north/north-westerly large scale flow as indicated by ECMWF analysis (not shown), possibly combined with local diurnal variations of the sea breeze (Johnson and Priegnitz, 1981). The initial convective cells developed vertically and then horizontally to form an anvil from its outflow (also named stratiform part of the convective system) in the

https://doi.org/10.5194/acp-2020-655
Preprint. Discussion started: 1 September 2020


Atmospheric Chemistry and Physics Discussions

upper troposphere driven off the coast by the easterly/south-easterly upper tropospheric flow.

Obs_Conv1 was already well developed at 05 UTC (13h local time: 13 LT) and was located around 5.5°N and 116°E at this time. Obs_Conv1 produced a large anvil on its west flank that started weakening after 10 UTC (18 LT). The anvil of Obs_Conv1 was well sampled by the Falcon aircraft during its mature stage at altitudes between 11 and 13 km from 8.05 UTC to 9.35 UTC (16.05 LT to 17.35 LT). The trajectory of the aircraft is plotted in Fig. 2 shows the intersection of the Falcon and the anvil cloud. The other convective cell, Obs_Conv2, initiated at 06 UTC (14 LT) and was located at about 4.3°N and 114.4°E. It later produced an anvil of convective outflow that developed and moved north-westward similarly to Obs_Conv1. It lasted several hours and started to decay from 10 UTC (18 LT).

The Falcon flight on the afternoon of November 19, 2011, was aimed at sampling the outflow of the Obs_Conv1 system. Krysztofiak et al. (2018) identified from humidity data and webcam images the times when the aircraft flew within the convective outflow (i.e., in cloudy conditions) and when it was in cloud-free conditions. This information has been used here to show in Fig. 2 where the flight sampled cloud-free air or cloudy air. It shows that the Falcon aircraft sampled the Obs_Conv1 system multiple times but also flew within the Obs_Conv2 system at ~12.5 km altitude around 9.20 UTC (visible at 5.2° N and 114.8° E) and in cloud-free conditions below Obs_Conv2 on its way back to Miri around 9.50 UTC at an altitude ~6 km. Since $CHBr_3$ emissions and its marine boundary layer (BL) mixing ratios are large close to Borneo's west coast (Ziska et al., 2013; Fuhlbrügge et al., 2016), it was expected that $CHBr_3$ would be transported from the BL aloft by the Obs_Conv1 and Obs_Conv2 systems. This scenario was confirmed by observations of elevated $CHBr_3$ mixing ratios relative to the background conditions during the flight (Sala et al., 2014; Krysztofiak et al., 2018). $CHBr_3$ measurements were performed by the GHOST instrument onboard the Falcon (Sala et al. 2014).

3 Model Simulations

3.1 Model Description

We use the Chemistry-Coupled Aerosol and Tracer Transport model to the Brazilian developments on the Regional Atmospheric Modeling System (C-CATT-BRAMS) (Longo et al. 2013), which is a version of the CATT-BRAMS model (Freitas et al., 2009) coupled on-line with a chemistry model. This system is capable of resolving meteorological processes and the resultant tracer transport and chemistry. C-CATT-BRAMS has its original heritage in the Regional Atmospheric Modeling System version 6 (RAMS) (Walko et al., 2000). RAMS is a fully compressible non-hydrostatic model consistent with Tripoli and Cotton (1982). RAMS can run in a nested grid configuration and includes various physical parameterizations to simulate sub-grid scale meteorological processes for turbulence, shallow cumulus convection, deep convection, surface-air exchanges, cloud microphysics, and radiation. BRAMS builds upon RAMS with the inclusion of several modifications that serve to improve the model performance within the tropics. For example, BRAMS includes an ensemble implementation of the deep and shallow cumulus convection schemes, a soil moisture initialisation using model prognostication combined with a remote sensing rainfall product, and more realistic surface characteristics for vegetation type derived from the MODIS NDVI

https://doi.org/10.5194/acp-2020-655
Preprint. Discussion started: 1 September 2020


Atmospheric Chemistry and Physics Discussions

product (Freitas et al., 2009).

The model represents microphysical processes using the single-moment bulk parameterization (Walko et al., 1995) whereby rain, cloud, pristine ice, snow, aggregates, graupel and hail are considered. The radiation scheme used in the model calculates the effects of clouds, hydrometeors, and aerosols upon radiation (Toon et al., 1989). The model considers turbulent mixing using the turbulent kinetic energy (mean kinetic energy per unit mass for eddies in turbulent flow) as a prognostic variable (Mellor and Yamada, 1982).

The chemistry scheme used in C-CATT-BRAMS simulates gas and aqueous phase chemistry, photochemistry, uptake described by Henry's Law, and hydrolysis. Marécal et al. (2012) and Krysztofiak et al. (2012) provide a detailed overview of the equations describing the chemistry solved by the model. To summarise, the model calculates chemical loss and production rates, and it computes chemical species concentrations in the gas phase, in cloud particles, and in rain droplets. To this end, the chemistry scheme couples with the microphysical scheme which explicitly resolves cloud and precipitation processes (Marécal et al., 2012). In practice, the model considers, within the bulk microphysical scheme, the effects on the chemical species of condensation, evaporation, water vapour deposition, and sedimentation. In addition, the reversible exchange of gases between the gas and aqueous phases (cloud and liquid hydrometeors) is estimated using Henry's Law and accommodation constants. Once within the condensed phase, the model includes the transfer of chemical species from within cloud particles to the different types of hydrometeors during coalescence and riming, and within the individual types of hydrometeor. In brief, it assumes Henry's law with cloud water and uses the production of precipitation to determine how much of the soluble trace gas is removed by wet deposition. We use retention coefficients to describe the proportion of a chemical compound that is retained in the condensed phase upon the transition from one type of hydrometeor to another. We simplify the treatment of retention for the formation of ice precipitates by assuming a retention coefficient of 1 (i.e., the entirety of the compound) for all chemical species dissolved in liquid precipitate that undergo freezing. This is a frequently used assumption within washout schemes in global and regional scale chemical models.

The photolysis rates are computed on-line in the model using the Fast-TUV radiative model (Tie et al., 2003). This is done in such a way as to consider the effects of clouds on photolysis rate in an interactive way.

The $BrONO_2$ hydrolysis reaction within cloud particles and rain droplets has been added to the chemical scheme. Its mathematical implementation is described by Marécal et al. (2012). The reaction scheme considers the reaction within cloud particles and rain droplets separately using the mean mass radius and mean mixing ratios for cloud particles and rain droplets from the bulk micro-physical scheme, the thermal velocity, the gas phase diffusivity, and the accommodation coefficient of $BrONO_2$.

3.2 New Model Developments

For the model to simulate chemical and physical processes associated with $CHBr_3$ degradation chemistry and its transport, several important changes had to be made to the model. A photochemical mechanism for the degradation of $CHBr_3$ was developed, tested, and optimised for use in C-CATT-BRAMS (Krysztofiak et al., 2012). The development of the new

https://doi.org/10.5194/acp-2020-655
Preprint. Discussion started: 1 September 2020

Atmospheric Chemistry and Physics Discussions

mechanism also included the estimation of the most favoured branching ratios for the halogenated peroxy reactions with the hydro-peroxy radical ($XRO_2 + HO_2$) (see Table 1 of Krysztofiak et al., 2012 for more details) using ab initio calculations of the standard reaction enthalpies. Reaction rates were either estimated from the analogous chlorine compounds or via a generalised expression. In addition, to properly simulate the uptake and washout of PGs into cloud particles and rain droplets, Henry's Law coefficients had to be estimated using predictive methods: the bond contribution method (Meylan and Howard, 1991) and the molecular connectivity index (Nirmalaklandan and Speece, 1988) for the brominated organic peroxides, CBr_3O_2H, $CHBr_2O_2H$, and the brominated carbonyl species, CBr_2O and CHBrO. Krysztofiak et al. (2012) discusses the validity of these estimates. The Henry's Law constants of bromine species are shown in Table 1. Note that the information on $BrONO_2$ is not included in Table 1 since it undergoes rapid hydrolysis in water and thus its removal is uptake limited (see Marécal et al. (2012) for details).

Table 1: Values used in the determination of the Henry's Law constants H_X[1] and effective Henry's constants H'_X[2] of bromine species X used in the model.

Species	H_{298} (mol l^{-1} atm^{-1})	a_H (K)	$K_{A\,298}$ (mol l^{-1})	H_X [1] *at cloud base (20 °C)*	H'_X [2] *at cloud base (20 °C) and cloud/rain pH of 5*
HBr	0.71[5]	10200[5]	1×10^{9} [4]	1.27	1.27×10^{14}
HOBr	6.1×10^{3} [3]	5900[4]	0	8.55×10^{3}	-
Br_2	0.76[5]	4177[5]	0	0.18	-
Br	1.7[3]	5200[3]	0	2.29	-
CBr_3OOH	1.96×10^{5} [6]	5200[7]	0	2.63×10^{5}	-
$CHBr_2OOH$	2.25×10^{4} [6]	5200[7]	0	3.03×10^{4}	-
CHBrO	74[6]	5800[8]	0	1.02×10^{2}	-
CBr_2O	21.5[6]	5600[8]	0	2.96×10^{1}	-
$CHBr_3$	3.4×10^{-2} [3]	1800 [3]	0	3.77×10^{-2}	-

[1] $H_X = H_{298} exp\left(a_H \left(\frac{1}{T} - \frac{1}{298}\right)\right)$

[2] $H'_X = H_X \times \left(1 + \frac{K_{A\,298}}{[H^+]}\right)$

[3]Sander (1999); [4]As for HOCl (Sander, 1999); [5]Yang et al. (2005); [6]Krysztofiak et al. (2012); [7]As for CH_3OOH (Sander, 1999); [8]Mean temperature dependency of RCHO and RR'CO (Sander, 1999)

These new developments coupled with a simple tropospheric chemistry scheme including carbon monoxide (CO), methane (CH_4), ozone (O_3), oxidised nitrogen (NO_y), and hydrogen oxide radicals (HO_x) (Barth et al., 2007) were successfully implemented by Marécal et al. (2012). Building on the new mechanism implemented in Marécal et al. (2012), non-methane

https://doi.org/10.5194/acp-2020-655
Preprint. Discussion started: 1 September 2020


Atmospheric Chemistry and Physics Discussions

hydrocarbon (NMHC) chemistry was added to the chemical mechanism in order to provide a more realistic description of the chemistry for the SHIVA real case study. The NMHC mechanism is a reduced version of the Regional Atmospheric Chemistry Mechanism (Stockwell et al., 1997) called Regional Lumped Atmospheric Chemical Scheme (ReLACS, Crassier et al., 2000). We term this modified version of the ReLACS scheme RELASH. RELASH includes 60 chemical species, 166 chemical reactions, treats NMHCs with up to 8 carbon atoms via lumping scheme, and is designed to describe tropospheric chemistry only. The full chemical mechanism is described in S1 of the supplement.

3.3 Model Configuration

The model simulation was run for 3 days from 12:00 UTC November 17 to 12:00 UTC November 20 2011. We used a nested grid configuration with three grids. The coarsest and largest grid covers from 90°E to 135°E and from 14°S to 23°N and uses a spatial resolution of 50 × 50 km; the next coarsest grid covers from 106°E to 123°E and from 2°S to 12°N at a resolution of 10 × 10 km; and the finest scale grid covers from 112.7°E to 117.4°E and from 3.3°N to 7.6°N and has a spatial resolution of 2 × 2 km. This horizontal spatial configuration allows the finest grid to completely include the two convective systems (Obs_Conv1 and Obs_Conv2) and the region covered by Falcon flight on the afternoon of November 19th. The finer domain and its associated model orography are plotted in Fig. 3. This illustrates well the abrupt topography on the west side of Borneo Island leading to the development of deep convection in sea-breeze conditions. The model has 53 vertical levels with varying vertical separation using finer resolution within the BL. The top of the model reaches to 26.6 km. The model meteorology was initialised and forced along the coarse grid boundaries of C-CATT-BRAMS using 6 hourly European Centre for Medium-Range Weather Forecasts (ECMWF) analysis fields for vector wind components, temperature, geopotential height, and specific humidity. We used the ECMWF operational analysis at 0.5°× 0.5° resolution.

Within the coarsest two model grids we enabled the parameterisations for shallow cumulus convection and for deep convection. We used the deep convection parameterisation from Grell and Dévényi (2002) as implemented in CATT-BRAMS in (Freitas et al., 2009). We allowed the model to resolve clouds and convective processes directly for the finest resolution grid. The topography used in the model has a 10 km resolution within the coarsest two grids and a 1 km resolution within the finest grid. Sea surface temperatures (SSTs) were initialised using the satellite observed weekly average SSTs (Reynolds et al., 2002).

To describe $CHBr_3$ emissions, we have implemented the emission inventory of Ziska et al. (2013). This is a bottom-up inventory based on the atmospheric and oceanic measurements of the HalOcAt (Halocarbons in the Ocean and Atmosphere) database project (https://halocat.geomar.de/). Using SHIVA flight measurements and the TOMCAT CTM, Hossaini et al. (2013) showed that this inventory performs best for bromoform in the Maritime Continent region compared to the inventories of Liang et al. (2010), Warwick et al. (2006) updated by Pyle et al. (2011), and Ordóñez et al. (2012). The Ziska et al. (2013) emissions have a 1° × 1° resolution. They are shown in Fig. 4 for the largest domain used in the C-CATT-BRAMS simulation. Note that the emissions are large on the west coast of Borneo Island where convection develops on the afternoon of November 19th, 2011.

Various chemical species were initialised and forced along the coarse grid boundaries using 6 hourly output from the TOMCAT

https://doi.org/10.5194/acp-2020-655
Preprint. Discussion started: 1 September 2020


Atmospheric Chemistry and Physics Discussions

CTM (Chipperfield, 2006). The chemical species were: $CHBr_3$, O_3, hydrogen peroxide, nitrogen oxide, nitrogen dioxide (NO_2), nitric acid, pernitric acid, CO, methane, ethane, propane, isoprene, HCHO, methaldehyde, ethaldehyde, acetone, peroxy actyl nitrate, peroxy propyl nitrate, methyl hydroperoxide, ethyl hydroperoxide, Br_2, BrO, HOBr, HBr, and $BrONO_2$, the bromo carbonyls $Br_2C(=O)$ and $HBrC(=O)$, and bromo peroxides ($CHBr_2OOH$ and CBr_3COOH). The TOMCAT simulation was run using the Ziska et al. (2013) emissions to ensure the consistency between the C-CATT-BRAMS simulation and its chemical boundary conditions from TOMCAT. For some of these species we had to perform lumping, splitting, and scaling by reactivity in order to achieve consistency with the chemical mechanism used in C-CATT-BRAMS.

4 Results

Consistent with the objectives of this paper, the results shown and discussed in this section are only those of the finest resolution grid (2 ×2 km, see Fig. 3) since it gives a detailed description of the meteorology and chemical composition within and in the vicinity of deep convection developing over the west coast of Borneo.

4.1 Meteorology

Simulations with limited area models with horizontal resolutions of the order of 1 km, as in the present study, are largely used to study in detail the development of convective systems since they provide an explicit representation of their dynamical and thermodynamic processes. At this resolution, there is no need to use sub-grid-scale parameterizations for convection. But even at this fine resolution, modelling tropical deep convective systems remains a challenge when one wants to reproduce the exact time, intensity and structure (extent of convective cloud component versus stratiform cloud component) compared to observations. This is particularly true in maritime conditions because of the uncertainties in the representation of hydrometeor properties and processes and because of their sensitivity to large scale meteorological conditions (e.g., Varble et al. 2014 and references therein). Instead, we now evaluate if the observed, general features of the development of the deep convective systems (described in Sect. 2 and Fig. 1) are well captured by the model. We do not attempt to make a detailed comparison of the model simulations with the particular convective systems sampled by the Falcon (Obs_Conv1 and Obs_Conv2).

To show the evolution of the modelled convective systems, we plot in Fig. 5 the simulated cloud top height derived by the simulation from 05 UTC to 12 UTC on November 19th, 2011. For this, we use the total condensed water field (the sum of liquid plus ice) to discriminate between cloud and cloud-free grid points with a threshold of 0.01 g kg^{-1} to filter out noise in the cloud ice field. Further, deep convection is very active at this time of the year, high thin cirrus clouds associated with earlier distant convection are also present in the simulation. Since cirrus can hide the development of deep convection occurring below, we add the condition that the model level below a grid box with cloud present must have a total condensed water mixing ratio > 0.025 g kg^{-1}. This threshold may lead to a slight underestimation of the cloud top height and horizontal extent of the convective systems. Therefore, Fig. 5 is mainly used here to show the general temporal and spatial development of the simulated convective systems but does not provide a precise measure of the cloud top height and spread of the anvil. Figure 5

https://doi.org/10.5194/acp-2020-655
Preprint. Discussion started: 1 September 2020

Atmospheric Chemistry and Physics Discussions

shows that the model simulates three deep convective systems that develop during the afternoon. These systems (called hereafter Mod_Conv1, Mod_Conv2 and Mod_Conv3) can be identified and followed in time by coloured rectangles. Consistent with the observations, the analysis of the simulated meteorological fields show that all three systems are triggered inland close to the coast in the early afternoon from the large-scale low-level winds (north/north-westerlies) enhanced by local sea-breeze that encounters the fairly steep topography of west Borneo (Fig. 3). This process is illustrated in Fig. 6a, which shows the simulated low-level wind direction and intensity at 06 UTC (14 LT, a time when convection is at an early stage) and the associated temperature field that exhibits a sea-land positive gradient. After 06 UTC the deep convective systems move offshore towards the west/north-west driven by the upper tropospheric winds, and they develop an anvil from their outflow. Upper tropospheric winds at 09 UTC (17 LT) are shown in Fig. 6b. Compared to the evolution of the observed brightness temperatures (Fig. 1), the vertical extension of the convective part of the systems during the mature stage tends to decrease a bit too rapidly in the model (Fig. 5), likely due to a too rapid removal of precipitation related to uncertainties in the microphysical parameters.

Table 2: Characteristics of the observed and simulated deep convective systems. The cloud top heights for the observed convective systems are based on Hamada and Nishi (2010) and Iwasaki et al. (2010). The outflow refers to the stratiform part of the convective system.

	Location where the convective system first reaches ~14.5 km altitude	Time when the convective system first reaches ~14.5 km altitude	Time when the outflow starts to dissipate	Estimated maximum top altitude of the outflow
Obs_Conv1	5.5°N-116.0°E	~5 UTC (~13 LT)	After 10 UTC (18 LT)	14.5 ±0.5 km at 9UTC (17 LT) 15.5 ±0.5 km at 10UTC (18 LT)
Obs_Conv2	4.3°N-114.4°E	~7 UTC (~15 LT)	After 11 UTC (19 LT)	15.5 ±0.5 km at 10UTC (18 LT) 14.5 ±0.5 km at 11UTC (19 LT)
Mod_Conv1	4.3°N-114.2°E	~5 UTC (~13 LT)	> 8 UTC (16 LT) (out of the domain)	~15.5 km at 7UTC (15 LT) ~15.5 km at 8UTC (16 LT)
Mod_Conv2	3.75°N-113.9°E	~8 UTC (~16 LT)	> 11 UTC (19 LT) (out of the domain)	~14.5km at 10UTC (18 LT) ~14.5km at 11UTC (19 LT)
Mod_Conv3	5.4 °N-115.8 °E	~8 UTC (~16 LT)	After 11 UTC (19 LT)	~14.5km at 10UTC (18 LT) ~14 km at 11UTC (19 LT)

The quantitative characteristics of the observed (Obs_Conv1, Obs_Conv2) and modelled (Mod_Conv1, Mod_Conv2, Mod_Conv3) convective systems are compared in Table 2. For Obs_Conv1 and Obs_Conv2, we use the estimates of the observed cloud top heights derived from brightness temperatures (Hamada and Nishi, 2010; Iwasaki et al., 2010) only where

https://doi.org/10.5194/acp-2020-655
Preprint. Discussion started: 1 September 2020


Atmospheric Chemistry and Physics Discussions

the uncertainty is ~0.5 km or lower. For the model, we use a set of cross sections from the 3D-fields to estimate the model cloud tops. Table 2 shows a general agreement on times and altitudes between the observations and the model.

Overall, from collating the information from Fig.1, Fig. 5, and Table 2, we find that the simulation represents the general characteristics of the observed convective systems well, in particular:

- the origin of their development from the interaction of the large-scale flow and the steep orography of the west coast of Borneo combined to local effects,
- the location of the initial convective cell about 30 km inland on the west coast of Borneo,
- the development of an anvil (the stratiform part) from the convective outflow during the afternoon moves off-shore,
- the cloud top height of the outflow,
- the transport of the convective systems north-westwards and westwards,
- the duration of the system of several hours and decay during early evening.

The main discrepancy is that the condensed water in the simulated convective part of the systems tends to precipitate a bit too efficiently compared to observations. Nevertheless, in its early stages, the convective part of the system, as evidenced by condensed water, reaches altitudes greater than 14.5 km. Achieving this altitude gives a strong indication that the intensity of the main updraft transporting bromoform into the upper troposphere is predicted well by the model.

In conclusion, the model is able to simulate the general meteorology of the observed convective systems, at least within the constraints and uncertainties of km-scale modelling of convection (Varble et al. 2014).

The three convective systems we examine detrain into altitudes ranging between 11 and 15 km. According to Corti et al. (2005) and Corti et al. (2006), the LZRH can be as low as 11 km for air masses within ice clouds due to the effects of their radiative properties. Ice clouds are present in the anvils of all three of the simulated systems, and they could cause a shift in the radiative balance and sufficient heating to lower the altitude of the LZRH. This would imply that the simulated air masses could gain positive buoyancy sufficient to reach the stratosphere over long enough time and large enough spatial scales. Thus, the study of the chemistry and washout within these systems could have relevance for the transport of $CHBr_3$ and its PGs to the stratosphere.

4.2 Bromoform Statistics and Convective Transport Efficiency

Before discussing the results of the simulated chemistry in detail (section 4.3), we evaluate if the simulation gives reasonable results for $CHBr_3$ concentrations compared to the aircraft observations. We use statistical characteristics for this comparison, and we do not make a direct comparison of the chemical species' mixing ratios along the flight track. We choose this approach for two reasons. First because of differences in location and timing between the observed and simulated convection events, and, second, because of spatial uncertainties in the emission inventory used in the simulation. This approach allows a clearer comparison of the observations and simulation by removing effects arising from inherent spatial uncertainties.

https://doi.org/10.5194/acp-2020-655
Preprint. Discussion started: 1 September 2020

Atmospheric Chemistry and Physics Discussions

In order to diagnose the convective transport efficiency for both observed and simulated systems we follow the approach proposed by Bertram et al. (2007) that was recently applied to study the SHIVA aircraft data (Krysztofiak et al., 2018). In order to estimate the air fraction, *f*, originating from the boundary layer (BL) and transported by convection we use the relationship:

$[X]_{UTconv} = f \,.\, [X]_{BL} + (1 - f) \,.\, [X]_{UTnoconv}$

where the mean mixing ratios in the boundary layer, the upper troposphere within the convective systems, and the upper troposphere in the vicinity but outside the convective systems are represented by $[X]_{BL}$, $[X]_{UTconv}$, and $[X]_{UTnoconv}$, respectively. Table 3 shows the modelled and observed mixing ratios of $CHBr_3$ that are used to calculate the *f* fraction. The mixing ratios are divided into three subsets corresponding to the boundary layer ($[X]_{BL}$), the upper troposphere within the convective systems ($[X]_{UTconv}$) and in the upper troposphere in the vicinity but outside the convective systems ($[X]_{UTnoconv}$). The details on how the estimates from the observations and from the model were determined are given in Appendix A.

Table 3: Estimates from the model simulations of the $CHBr_3$ mixing ratios in the boundary layer $[X]_{BL}$, in the UT outside convection $[X]_{UTnoconv}$ and in the UT within convection $[X]_{UTconv}$. *f* is the air fraction originating from the boundary layer and transported by convection. Details on the method used are given in Appendix A. (*) corresponds to the SHIVA estimate from 4 flights and boat data from different days including the flight on the afternoon of November 19, 2011, using measurements of different species ($CHBr_3$, CO, CH_4, and CH_3I) (Krysztofiak et al., 2018).

	$[X]_{BL}$ (mean ± 1σ)	$[X]_{UTnoconv}$ (mean ± 1σ)	$[X]_{UTconv}$ (mean ± 1σ)	fraction *f*
Mod_Conv1	2.11 ± 0.24	0.29 ± 0.07	0.62 ± 0.18	0.18 ± 0.11
Mod_Conv2	1.20 ± 0.25	0.33 ± 0.13	0.62 ± 0.13	0.33 ± 0.23
Mod_Conv3	1.58 ± 0.37	0.34 ± 0.11	0.56 ± 0.12	0.18 ± 0.14
Obs_Conv1 and Obs_Conv2 from $CHBr_3$ SHIVA observations on the afternoon of November 19th, 2011	1.82 ± 0.86	0.51 ± 0.04	0.73 ± 0.12	0.17 ± 0.15
Mean from observations of 4 SHIVA flights*				0.29 ± 0.25

Mod_Conv1 and Mod_Conv3 give values of the fraction of air transported by convection from the BL that are close to the estimates of *f* based on $CHBr_3$ observations gathered on November 19th, 2011.

A higher *f* fraction is calculated for Mod_Conv2 meaning that this system was more efficient for transport of $CHBr_3$ from the BL to the UT. However, this high fraction *f* is consistent with the average value calculated from all SHIVA aircraft data (0.29 ± 0.25) determined by (Krysztofiak et al., 2018) using carbon monoxide measurements from the SPIRIT instrument (Catoire et al. 2017) and the GHOST $CHBr_3$ measurements onboard the Falcon (Sala et al., 2014). Table 3 shows an overall good consistency (both in terms of magnitude and simulated variability) between the model results, the findings of Krysztofiak et

https://doi.org/10.5194/acp-2020-655
Preprint. Discussion started: 1 September 2020


Atmospheric Chemistry and Physics Discussions

al., (2018), and the SHIVA measurements concerning *f*. Furthermore, Fuhlbrügge et al. (2016) used a trajectory model and found similar values of *f* at 10-13 km of between 30-40% for November 19th for the west coast Borneo region.

We now examine the magnitude of the $CHBr_3$ mixing ratios in the BL and in the UT in both inside and outside of the convection using Table 3 and Figure 7. The box and whisker plots in Figure 7 provide complementary statistical information on the observed and simulated $CHBr_3$ mixing ratios.

In the BL, the Mod_Conv1 mean mixing ratio is higher compared (~22% higher in terms of the median, see Fig. 7; ~16% higher in terms of the mean, see Table 3) to the observations. Meanwhile, the mean mixing ratio in the BL below Mod_Conv3 is a bit lower than that observed, and Mod_Conv2 shows the lowest mean there (Table 3). This is likely related to two combined factors: the emissions are weaker in the southern part of Borneo's west coast where Mod_Conv2 takes place (see Fig. 4); and Mod_Conv1 initiates in closer proximity to the coast compared to the other two systems where $CHBr_3$ emissions and BL mixing ratios are higher. In the BL, there is a large spread in the observations because of the very large local variability of the emissions that the model cannot capture due the resolution of the $CHBr_3$ emission inventory we used. Nevertheless, the median BL mixing ratios of all three lie within the 25th and 75th percentile of the observed BL mixing ratios, and the entire range of simulated mixing ratios across all three simulated systems lie within the complete range of observed mixing ratios in the BL.

The mean background UT (UT_{noconv}) mixing ratios in the simulation, which largely depend on the chemistry initial conditions from the TOMCAT simulation, are underestimated, which leads to lower mixing ratios both within and out of the convection (differences of 0.17 to 0.22 pptv in UTnoconv, and of 0.11 to 0.17 pptv in UTconv). Hossaini et al. (2013) previously showed a comparable 0.08 pptv average negative bias in TOMCAT relative to the SHIVA aircraft measurements of $CHBr_3$ throughout the entire duration of the flight on the afternoon of November 19th. If we consider the higher spatial resolution of our simulations and the smaller domain considered for the statistics compared to TOMCAT, these remaining differences appear consistent with one another.

In the UT, the underestimate in $CHBr_3$ mixing ratio is more pronounced outside of the convection, which we suspect is linked to an underestimate in the emissions somewhere to the East of Borneo where these background UT air masses originate from in the TOMCAT simulation. This finding is consistent with Fuhlbrügge et al. (2016) who showed that local sources alone cannot account for the observed $CHBr_3$ levels in the UT. Furthermore, Keber et al. (2020) indicate that underestimates in the background tropical UT might arise due to underestimates in extratropical $CHBr_3$ sources. Meanwhile, the simulated mixing ratios in the UT affected by convection (UT_{conv}) are a much more direct measure of the emissions along the west coast of Borneo and are simulated by C-CATT-BRAMS. Background UT air mixes within the convective outflow during the detrainment process in the UT. This mixing process could explain why mixing ratios simulated within the convective outflow are slightly lower than observed $CHBr_3$.

In the background UT (UT_{noconv}), we see small differences in the mixing ratios in the vicinity of the three simulated convective systems with slightly higher values and variability for Mod_Conv2 and Mod_Conv3 because they developed in locations

https://doi.org/10.5194/acp-2020-655
Preprint. Discussion started: 1 September 2020


Atmospheric Chemistry and Physics Discussions

previously affected by convective transport of bromoform. The three convective systems show similar results for $[X]_{UTconv}$ though with a higher variability in Mod_Conv1 related to a more elongated horizontal extent of the anvil (see Fig. 5).
Note that the results presented in this section have little sensitivity to the threshold in ice concentration used to define the sampling of grid points within the convection and outside in its vicinity (see Supplement S2).

4.3 Cross section analyses of the simulated chemical processes

4.3.1 Bromoform

In this section, we analyse the cross sections of the simulated chemical fields of $CHBr_3$ within the convective systems. As an illustration of how $CHBr_3$ evolves during the convection, Fig. 8 shows a vertical cross section of the 5-hour time evolution of $CHBr_3$ mixing ratios in the central part of the Mod_Conv3 system, together with contours of total condensed water from cloud and precipitation to locate the convective ascent and associated outflow. We selected Mod_Conv3 since it corresponds mostly close in space to Obs_Conv1. We can see the complete evolution of the convective system from a situation with elevated $CHBr_3$ concentrations in the boundary layer close to the location of the convection (of up to 2.1 pptv) at the very early stage of the system. Then the convective column ascends in a relatively vertical fashion and afterwards develops an anvil on its west side. The concentrations in the anvil are naturally highest closest to the point of convective detrainment and reach up to 0.9 pptv at 9 UTC (17 LT) and begin to decrease after one hour (up to 0.75 pptv) as the anvil is advected north westward by the high-altitude winds.
The analysis of the transport, chemical processes, and Br-atom speciation done hereafter is based on vertical cross sections chosen in the central part of each convective system at the time when the anvil is in its mature stage; the precipitation and vertical transport within the convective column are also near their maximum at this stage. This means that these cross sections are representative of the most intense convective activity which demonstrate the combined effects of intense vertical transport, washout, and development of the anvil. All of the numbers presented in the following sections correspond to those of the cross-sections presented in the figures. Also, to be able to compare the contribution of the different bromine species to the total Br-atom mixing ratios all the figures hereafter are expressed as Br-atom mixing ratios (henceforth known as pptv Br).
We show the concentrations of $CHBr_3$ in the three convective systems in Figs. 9 (a), (b), and (c). Each of the three simulated convective systems exhibit different $CHBr_3$ mixing ratios within their convective columns and within their outflow anvils. This variability is because they each entrained different boundary layer mixing ratios of $CHBr_3$, and they also detrained into UT regions with slightly differing $CHBr_3$ backgrounds and have different transport efficiencies (Table 3).
Despite these variations, we see a consistent result in the Br-atom speciation and mixing ratios of each convective system in Figs. 9 and 10 (expressed as the percentage of contribution). $CHBr_3$ is elevated above background levels in all of the atmospheric regions dynamically linked to the boundary layer (surface to 600-800m height) on a timescale well below the lifetime of $CHBr_3$ (i.e., the boundary layer, convective columns, and convective outflow). We can see that the $CHBr_3$ in these air masses has only undergone limited photochemical ageing because $CHBr_3$ accounts for >85% of the total Br mixing ratio

https://doi.org/10.5194/acp-2020-655
Preprint. Discussion started: 1 September 2020


Atmospheric Chemistry and Physics Discussions

(Figs. 10 (a), (b), and (c)) in these atmospheric regions. However, we consistently see lower $CHBr_3$ contributions to the total Br mixing ratio in atmospheric regions above the boundary layer not affected either directly or indirectly by convection. These regions include the low (from the top of the boundary layer to ~2 km height), mid (from ~2 km height to ~8 km) and upper-troposphere (from ~8 km height to ~13-14 km) where the model typically simulates 0.45-0.9 pptv Br of $CHBr_3$ accounting for 60-70% of the total Br mixing ratio in the absence of convection to any vertical level. We can see some evidence of elevated $CHBr_3$ in the upper troposphere related to the transport of outflow from distant convection, for instance in Fig 9 (c) at around 116.5° E longitude and at 11 to 12 km. Within these air masses the model simulates intermediate mixing ratios and Br-atom contributions signifying air masses of intermediate $CHBr_3$ ageing and mixing. Note that the sharp changes in bromine mixing ratios that we see above 14 km in Figs. 9 and onwards are due to the vertical transition into the tropical tropopause layer, which is influenced by the stratosphere where we find 0-0.45 pptv Br of $CHBr_3$ accounting for 15-20 % of the total simulated Br mixing ratio there.

4.3.2 Inorganic and Organic PGs

Figs. 9 (d), (e), and (f) show that there are relatively low levels of inorganic bromine (Br, Br_2, BrO, HOBr, HBr, $BrONO_2$) concentrations in the lowest areas of the boundary layer even in the areas not directly affected by convective precipitation with values typically in the range of 0 to 0.4 pptv Br, i.e., <5 % contribution to the total Br mixing ratio in the boundary layer. The highest simulated inorganic bromine mixing ratios (0.3-0.4 pptv Br) in the boundary layer occur to the west of the Mod_Conv3 system still only contributes <10 % to the total boundary layer pptv Br (see Fig. 10 (f)). This spatial variability in the boundary layer inorganic bromine mixing ratios around each convective system arises due to differences in precipitation location and timing over the course of the simulation prior to November 19th, 2011. Precipitation events occurring in the two preceding days deplete the boundary layer of inorganic bromine due to washout (analysis not shown). Inorganic bromine concentrations are enhanced in the lower free troposphere between 1 and 4 km to the west of each convective system (Figs. 9 and 10 (d), (e), and (f)). There, total inorganic PGs peak up to 1 pptv Br, which constitutes a sizeable portion (up to 45%) of the total Br mixing ratio. Meanwhile, air masses in the convective column itself and convective outflow are almost entirely depleted of inorganic bromine with mixing ratios of <0.1 pptv Br and with contributions to the total Br mixing ratio well below 5%.
The highest bromine mixing ratios from organic PGs (CHBrO, CBr_2O, $CHBr_2OOH$, and CBr_3COOH) are found mainly in the BL and lower troposphere (i.e., up to 0.2 pptv Br) where PGs are formed due to $CHBr_3$ photochemical loss (Figs 9 and 10 (g), (h) and (i). Furthermore, we can see that within the convective systems, organic compounds are being driven from the low levels up to the upper troposphere in the main ascent and the outflow and show enhanced mixing ratios within the convective column compared to the free troposphere. Nevertheless, organic bromine exhibits much lower pptv Br compared to $CHBr_3$ overall, and the contribution from the organic PGs is lower than the inorganic compounds within the lower troposphere above the BL away from convective systems. Among the three convective systems, Mod_Conv3 exhibits the highest concentrations of the organic PGs and relative contributions west of the convective system below 2.5 km in altitude. However, their relative

https://doi.org/10.5194/acp-2020-655
Preprint. Discussion started: 1 September 2020


Atmospheric Chemistry and Physics Discussions

contribution generally remains below 5% between the BL top and 5 km in altitude and around 1-2% within the convective systems and the outflow.

4.3.3 The Impact of PG Solubility

Given that washout is an important process within the convective systems, the relative solubilities of each component we look at is relevant for explaining the concentration levels of the inorganic and organic PGs. Table 1 shows the Henry's Law constants for the PGs. In order of increasing solubility, we first list the inorganic bromine PGs: BrO, Br, Br_2, HOBr, HBr, $BrONO_2$; and then the organic PGs: CHBrO, CBr_2O, $CHBr_2OOH$, and CBr_3COOH. In discussions from this point on, we will classify the inorganic PGs into two groups: soluble inorganic that includes HOBr, HBr, and $BrONO_2$; and insoluble inorganic, comprising Br, Br_2, and BrO. We also classify the bromo-carbonyls as insoluble organic and the bromo-methyl peroxides as soluble organic PGs. Note, that except for Br_2, $CHBr_3$ is insoluble relative to its PGs.

The gas phase mixing ratios of soluble inorganic bromine species are depleted to near zero in the convective columns and in the immediate area of detrainment for each system (Fig.11, a-c). Similarly, soluble inorganic species make almost no contribution to the total gas phase Br within each convective system (Fig. 12, a-c). This depletion of soluble inorganic bromine species occurs even though their boundary layer mixing ratios range between 0.1 and 0.5 pptv Br and the soluble inorganic species form the bulk of the inorganic bromine at all levels in the troposphere outside of convective systems. This strongly implies that the model simulates the near total removal of the soluble inorganic bromine species within the convective columns. The insoluble inorganic species (Figs. 11 and 12 (d), (e), and (f)) only make a negligible contribution to the total bromine budget throughout the troposphere, only reaching peak mixing ratios of 0.1 pptv Br and 4% of the total bromine in areas of the lower troposphere not affected by convection. We also see no enhancement of the insoluble inorganic species (which include Br_2) within the convection column or in the fresh convective outflow above the levels seen in the rest of the troposphere. There is also only a negligible contribution of insoluble inorganic bromine in the UT affected by previous convection as illustrated in Figs. 12 (e) and (f) (to the East of both Mod_Conv2 and Mod_Conv3).

The contribution to the total Br mixing ratio from the soluble organic bromine PGs is also negligible (at a maximum of ~1% in the low troposphere not affected by convection). The bulk of organic PG species are instead in the form of insoluble species. The enhancements of the organic PGs we see in the convective system (up to 0.08 pptv compared to 0.02 pptv) in Figs. 9 (g), (h), and (i) are due to the insoluble bromo-carbonyls. These compounds contribute 86% of the PG bromine total.

In order to understand further the behaviour of inorganic bromine we need to examine its composition. HBr dominates the inorganic Br-atom contribution in the regions of the UT outside of the convective systems (Figs. 13 (a) to (c)). It provides between 40-65% of the total Br mixing ratio in the regions of the low and mid-troposphere (1.5-4 km height) unaffected directly by precipitation washout (Fig. 14, a-c) while HOBr represents just a small fraction (0-35%) of the remainder (Figs. 13 and 14 d-f). The lower to mid-troposphere (1.5-4 km) is the only tropospheric region where HOBr has significant mixing ratios of up to 0.3 pptv. Otherwise HBr dominates the total inorganic Br mixing ratio in the BL and UT. Note that HBr and HOBr

https://doi.org/10.5194/acp-2020-655
Preprint. Discussion started: 1 September 2020


Atmospheric Chemistry and Physics Discussions

contributions within the most active part of the convective systems are not meaningful since the total inorganic bromine levels are negligible there.

4.3.4 Discussion

A key finding is that inorganic bromine dominates the PG budget within the troposphere, yet despite this the inorganic PGs are almost entirely removed during convective transport by washout due to their solubility. We here argue that the regional tropospheric composition present in our simulations is the underlying cause of this prevalence of HBr and in turn the washout of inorganic PGs that results from this.

Within the photochemical scheme of C-CATT-BRAMS, bromine atoms can react in the gas phase in one of three ways.

$Br + O_3$ - > $BrO + O_2$ (R1)

Br + HCHO -> HBr (R2)

$Br + HO_2$ -> HBr (R3)

Probably of most significance in the troposphere, bromine atoms can react with ozone via R1 to form BrO. However, under relatively low ozone conditions, reactions R2 and R3 can begin to dominate the reaction budget for Br-atoms favouring the formation of HBr instead of BrO. This has important implications for the washout of Br within convective systems because HBr is extremely soluble but BrO is very insoluble.

The maritime continent has been noted for having low O_3 levels throughout the depth of the troposphere during the winter monsoon resulting from westward transport of moist tropical air across the equatorial Pacific (Rex et al., 2014). The relatively low ozone levels are reproduced in our simulations (daytime values of as low as 10-15 ppbv at 2 km) and arise from the same mechanism across the equatorial Pacific represented in the TOMCAT global model forcing. This favours the formation of HBr and therefore this enhances the removal of inorganic bromine within the simulated convective clouds systems we study here.

The low levels of BrO have another implication. BrO is also an important precursor for other key inorganic bromine compounds in the troposphere.

$BrO + HO_2 \rightarrow HOBr$ (R4)

$BrO + NO_2 \rightarrow BrONO_2$ (R5)

$BrONO_{2(aq)} \rightarrow HOBr_{(g)} + HNO_{3(g)}$ (R6)

BrO is directly involved in the two chemical pathways leading to HOBr formation; either the direct formation pathway via R4 or via the two-step pathway involving the formation (R5) and then hydrolysis of $BrONO_2$ (R6). Thus, the low levels of BrO can be implicated in the lack of significant quantities of HOBr (Figs. 13 and 14). This has another implication: HBr and HOBr react with one another in the aqueous phase to produce Br_2 via reaction R7.

$HOBr_{(aq)} + Br^-_{(aq)} + H^+ \rightarrow Br_{2(aq)} + H_2O$ (R7)

Since this reaction has a stoichiometry of 1:1, and our model simulates that HBr is in a vast excess compared to HOBr in the troposphere, HOBr is the limiting reactant for Br_2 formation.

https://doi.org/10.5194/acp-2020-655
Preprint. Discussion started: 1 September 2020


Atmospheric Chemistry and Physics Discussions

The atmospheric implication of R7 is that two soluble gases (HBr and HOBr) could potentially react rapidly within cloud and rain droplets to form the insoluble gas Br_2. R7 is known to lead to the production and release of significant quantities of Br_2 in other environments combining both the aqueous and gas phases, e.g., in the polar ice regions (McConnell et al., 1992) and within volcanic plumes (Oppenheimer et al., 2006). In these examples the gas phase and aqueous phase chemistry combine to form a feedback loop leading to what is known as the "bromine explosion" (Wennberg, 1999). Thus, R7 could have the potential to significantly alter the Br-atom speciation within convective clouds in a short time in such a way as to reduce the PGs overall solubility; this would therefore promote the vertical transport of Br-atoms within convective systems even in the presence of abundant falling hydrometeors that would otherwise washout soluble gases like HBr very rapidly. In our simulation, only negligible levels of Br_2 form during the most active phase of each of the simulated convective systems (Fig. 15). At most we see up to 0.04 pptv of Br_2 within Mod_Conv3, and this is only within the lowermost sections of the system and these levels do not propagate vertically into the UT.

From this analysis, we should expect more production of Br_2 in convective systems in environments with higher levels of background ozone, which would consequently have more HOBr. A further reason is that the hydrometeors containing the dissolved HBr and HOBr simply fall fast leading to a very short residence time that prevents their concentrations from accumulating to the point where R7 becomes important.

While other studies exist of convective scale modelling of ozone and aerosols (Crumeyrolle et al., 2008; Tulet et al., 2002), Marécal et al. (2012) is the only other study to have simulated the transport and photochemistry of bromoform at the convective scale and so we therefore compare our findings with that study. Marécal et al. (2012) showed in their analysis of simulations of an idealized case study of a tropical deep convective system that most of the Br transported to the UT by convection is in the form of $CHBr_3$, which is consistent with the results here. Nevertheless, in their case using an initial $CHBr_3$ of 1.6 pptv in the BL (which is the most comparable to this study), we can see notable differences in the composition of the convective outflow. Both organic and inorganic PGs are in higher abundance within the upper reaches of each convective system in this study compared to Marécal et al. (2012). In particular, the mixing ratios of all the inorganic PGs are greatly increased by over a factor of ten here compared to Marécal et al. (2012). As a result, Marécal et al. (2012) found a higher relative contribution to the total bromine PG mixing ratio in the UT for organic with respect to inorganic PGs, i.e., 86 % compared to 46% in this present study. The background tropospheric air contains elevated HBr levels in our simulation (Fig. 13 and 14) resulting from photochemical ageing of convectively lofted $CHBr_3$ represented both within the TOMCAT CTM initial and boundary conditions. In Marécal et al. (2012), the initial conditions are such that $CHBr_3$ is mainly below 2 km and there is no $CHBr_3$ above 5 km altitude. Furthermore, they used a PG background of zero in the mid to upper troposphere. Thus, we can conclude that the major differences in simulated inorganic and organic PG mixing ratios within the convective system arise as a result of the idealized PG background and initialization used within Marécal et al. (2012) compared to the more realistic simulation of the PG background (specifically HBr) in this study.

Another difference is that the simulations in Marécal et al. (2012) are set over Darwin as opposed to Borneo. The small difference in latitude and atmospheric conditions is enough to cause longer $CHBr_3$ lifetimes in our simulation with respect to

https://doi.org/10.5194/acp-2020-655
Preprint. Discussion started: 1 September 2020


Atmospheric Chemistry and Physics Discussions

both photolysis (15.2 days compared to ~19 days here) and OH (22.6 days compared to 52.6 days here). Overall, both processes contribute to an increase in $CHBr_3$ lifetime from 9 to ~14 days here (note both are fully consistent with the compiled ranges from Burkholder et al., 2018). The relative importance of photolysis has therefore increased in this study due to these changes, which could lead to an increase in the relative formation rates of inorganic bromine PGs compared to the organic PGs. This occurs because the photolysis of bromine cleaves off single bromine radicals that then contribute directly to the inorganic PG budget. Furthermore, the remaining organic PGs contain one fewer bromine atoms as a result. Meanwhile, reaction with OH leads to the abstraction of a hydrogen atom, which creates organic PGs containing either two or three bromine atoms. Given the idealized initialization and experimental design within Marécal et al. (2012), it is not possible to properly assess these conjectures here, but it would be of interest to evaluate more formally differences in PG speciation arising in different photochemical environments that display differences in the $CHBr_3$ lifetime with respect to reaction with OH and to photolysis. Also, Marécal et al. (2012) showed that significant Br_2 can be released into the gas phase via aqueous processes in cloud droplets, but only when their idealized simulation was initialized with very high $CHBr_3$ (40 pptv) in the BL. In the more realistic case study simulated here where boundary layer $CHBr_3$ is ~2 pptv, we find that the production of Br_2 via R7 also takes place but is a negligible contribution to the total inorganic bromine as shown in Fig. 15. This is consistent with the results of Marécal et al. (2012) when using only 1.6 pptv as the initial $CHBr_3$ in the boundary layer. This is because the simulations in Marécal et al. (2012) took place near Darwin where there was also still a relatively low O_3 background (14 ppbv at 2 km).

5 Limitations

There are a few limitations to this study. First, it could be difficult to generalise these results to other tropical areas because we studied a region with a relatively low ozone background in the troposphere, which impacts the tropospheric bromine chemistry. Furthermore, other tropical regions could have vastly different $CHBr_3$ emissions, and in the case of much higher emissions, as was explored in Marécal et al., (2012), we could expect a larger role for Br_2 formation. We also neglect other VSLS in our simulations and only focus on $CHBr_3$, and as a result our findings are specific for the case where $CHBr_3$ is the only VSLS. Including other VSLS would alter the relative contributions made by $CHBr_3$ and its PGs to the vertical transport of bromine to the UT.

Another limitation is that our analysis is performed on cross sections of the most mature convective systems, and so our analyses offer a snapshot of the most intense convective activity and its effects.

Lastly, the performance of the various top-down and bottom-up $CHBr_3$ inventories varies significantly by region and the divergent global emission estimates represent a significant source of uncertainty in estimates of strat-Br_y^{VSLS} (Hossaini et al., 2013). Despite the difference in simulated $CHBr_3$ mixing ratios that we identify in the background UT we argue that the choice in using the Ziska et al. (2013) emission inventory was the correct one. Here, we cite Hossaini et al. (2013) that determined that the Ziska et al. (2013) emissions gave the closest agreement to observations when evaluated in the TOMCAT CTM over the same region of Borneo. Indeed, our results show consistent $CHBr_3$ mixing ratios compared to the simulations of Hossaini

https://doi.org/10.5194/acp-2020-655
Preprint. Discussion started: 1 September 2020


Atmospheric Chemistry and Physics Discussions

et al. (2013) for the November 19th flight. Furthermore, Ziska et al. (2013) project a $CHBr_3$ emission climatology ranging between 1200-1600 pmol m^{-2} hr^{-1} within the region of interest along the north west coast of Borneo while the emissions measured locally (over several days) by Fuhlbrügge et al. (2016) range from 300-4300 pmol m^{-2} hr^{-1}. We conclude from this that Ziska et al. (2013) provides a good estimate of $CHBr_3$ emissions over this specific area.

6 Summary and Conclusions

We used a convective scale model (2 × 2 km resolution) in order to gain a better understanding of the effects of tropical deep convection on the transport of $CHBr_3$ and the speciation of its PGs in the troposphere. Until now, two modelling studies have been carried out at the convective scale but only for idealised cases (Krysztofiak et al. 2012, Marécal et al., 2012). Our objective was to go a step further by modelling a real case study of deep convection that occurred along the west coast of Borneo on the afternoon/early night of 19 November, 2011, during the SHIVA field campaign.

It was shown that the meteorological development of the convective systems in the model have general characteristics similar to those observed. We compared our modelled $CHBr_3$ mean concentrations and convection transport efficiency to those derived by Krysztofiak et al. (2018) from SHIVA measurements. The comparison showed an underestimation of the $CHBr_3$ background concentrations within the upper troposphere related to underestimates in the Ziska et al (2013) emissions to the East of Borneo. These findings are consistent with those of Keber et al. (2020) that showed similar underestimates in the background tropical UT and with Fuhlbrügge et al. (2016) that showed that local sources alone cannot account for the observed $CHBr_3$ levels in the UT. Nevertheless, the fraction *f* of air from the BL driven in the UT by the convective systems is consistent with Krysztofiak et al. (2018): 0.18±0.14 to 0.33±0.23 for the model and 0.17±0.15 to 0.29±0.25 for the observations.

Despite variation in the timing, location, and availability of $CHBr_3$ for entrainment in the BL below each convective system, the same general behaviour is observed across all three simulated convective systems. Most of the bromine (>85%) transported to the UT in each convective system is in the form of $CHBr_3$. Within the convective systems, the remaining 1-2% of the total bromine present is mostly in the form of organic PGs, i.e., the insoluble brominated carbonyls CHBrO and CBr2O (86% as a contribution to the total PG). This is despite the inorganic PGs making a larger contribution than the organic PGs to the total Br mixing ratios in the free troposphere (i.e., 45% versus only 5%). Falling hydrometeors within the convective column efficiently remove the inorganic PGs, whose tropospheric budget is dominated by the extremely soluble HBr gas. Overall, we conclude that organic PGs are more important than inorganic PGs for the vertical transport of bromine within the convective columns for the conditions that we study here.

The insoluble inorganic PGs, BrO and Br_2, are only present at negligible mixing ratios and play no significant role in the vertical transport of bromine. Our interpretation is that the tropospheric inorganic PG budget is shifted heavily in favour of HBr formation due to the low background O_3 mixing ratios simulated in this region. This limits the availability of HOBr leading to only very limited formation of Br_2 within the cloud and rain droplets within the convective system resulting from the reaction between HBr and HOBr. More BrO and HOBr would form in cases with higher background O_3, which would lead

https://doi.org/10.5194/acp-2020-655
Preprint. Discussion started: 1 September 2020


Atmospheric Chemistry and Physics Discussions

to enhanced Br_2 formation within convective systems and a more important role of the inorganic PGs for the vertical transport of bromine.

Overall, these conclusions are valid in all parts of the convective system except for where the anvil detrains into residual convective outflow in the UT. In this case, the Br speciation within and around the anvil is perturbed with increases in the background UT $CHBr_3$ and PGs produced by photochemical ageing of the $CHBr_3$ within the UT. Thus, the exceptions to our conclusions are due to factors external to the systems themselves.

7 Outlook

It would be of interest to evaluate findings from global CTM studies of VSLS transport to the UT and stratosphere in light of our findings based on modelling at the convection scale. This additional work, however, is beyond the scope of this study since it would require considerable additional technical work to reconcile the differences in spatial scale and conditions since global CTMs derived grid scale mixing ratios representing the mean both within and outside of convective systems. We hope to reconcile these issues and test the hypotheses raised in this paper as part of future work. This future effort could provide insights into the processes represented within CTMs.

Appendix A

Here are the details on how we calculated the simulated and observed mixing ratios presented in Table 3. Following Krysztofiak et al. (2018), the mean mixing ratio estimates based on Falcon measurements for the $[X]_{UTconv}$ and $[X]_{UTnoconv}$ (~11-13 km altitude range) were split according to humidity data and webcam images corresponding to cloudy or cloud-free conditions, respectively. $[X]_{BL}$ are data gathered during the flight ascent/descent from/to Miri between the surface and 400 m height combined with Sonne ship measurements (Fuhlbrügge et al., 2016) close to the convective system.

The estimates from the simulations are calculated similarly for each of the modelled convective systems and in a manner as consistent as possible with Krysztofiak et al. (2018). For $[X]_{UTconv}$ and $[X]_{UTnoconv}$, a box of 1°x1° and 11-13 km altitude is selected around the convective system and $[X]_{UTconv}$ are selected where cloud ice is present. We use two different ice concentration thresholds to define both the air masses within the anvil cloud and those outside of it: a cut-off of 0.01 g kg^{-1} to define air masses within the cloud, and 0.005 g kg^{-1} to define those outside of it that are part of the simulated upper tropospheric background. We use two thresholds to define these separate air masses to ensure we derive an adequate separation between the two; air masses lying between the lower and upper cut-off show mixing and dilution of the convective outflow and neither represent background or convective outflow concentrations in a clear way. To demonstrate the sensitivity of our results to this choice, we perform a sensitivity test with two different single ice concentration thresholds to define air inside or outside the convective cloud: 0.01 g kg^{-1} and 0.005 g kg^{-1}. These results are presented in the supplement S2. For $[X]_{BL}$, a box of 0.5° × 0.5° and 0-400 m altitude is selected around the area where the initial convective cell starts its development. For each system,

https://doi.org/10.5194/acp-2020-655
Preprint. Discussion started: 1 September 2020

Atmospheric Chemistry and Physics Discussions

two model outputs one hour apart were selected during the main phase of the outflow development for $[X]_{UTnoconv}$ and $[X]_{UTconv}$, and at the times when the initial convective cell starts developing for $[X]_{BL}$. The times and boxes chosen are given in Table A1.

Table A1: Times and latitude/longitude boxes used to calculate $[X]_{BL}$, $[X]_{UT}$ and $[X]_{UTconv}$ on November 19, 2011.

	$[X]_{BL}$ time	$[X]_{BL}$ box	$[X]_{UTnoconv}$/$[X]_{UTconv}$ time	$[X]_{UTnoconv}$/$[X]_{UTconv}$ box
Mod_Conv1	4 UTC 5 UTC	4.2°N - 4.7°N 114.0°E - 114.5°E 4.2°N - 4.7°N 114.0°E - 114.5°E	6 UTC 7 UTC	4.1 - 5.1°N 113.3°E - 114.3°E 4.3°N - 5.3°N 113.0°E - 114.0°E
Mod_Conv2	7 UTC 8 UTC	3.35°N - 3.85°N 113.55°E - 114.05°E 3.35°N - 3.85°N 113.55°E - 114.05°E	9 UTC 10 UTC	3.25°N - 4.25°N 113.1°E - 114.1°E 3.25°N - 4.25°N 112.9°E - 113.9°E
Mod_Conv3	7 UTC 8 UTC	5.1°N - 5.6°N 115.8°E - 116.3°E 5.1°N - 5.6°N 115.8°E - 116.3°E	9 UTC 10 UTC	5.3°N - 6.3°N 115.3°E - 116.3°E 5.0°N - 6.0°N 114.9°E - 115.9°E

Author contributions.

PDH: co-designed the study, wrote the main text of the paper, ran the model, analysed the model results, and created many of the figures.

VM: co-designed the study, helped develop this version of C-CATT-BRAMS, wrote some of the text, and created some of the figures.

RH: ran the TOMCAT simulations and helped edit the manuscript

MP: co-designed the chemical mechanism and the study, helped develop this version of C-CATT-BRAMS

GK: co-designed the chemical mechanism, helped develop this version of C-CATT-BRAMS, and edited the manuscript.

FZ: developed the emissions and provided us with the emission data.

AE: headed the GHOST-MS team onboard the Falcon aircraft and helped to edit the manuscript.

SS: a member of the GHOST-MS team onboard the Falcon aircraft.

TK: a member of the GHOST-MS team onboard the Falcon aircraft.

HB: a member of the GHOST-MS team onboard the Falcon aircraft.

EA: collected the CHBr3 observations on the Sonne boat cruise during SHIVA.

MC: helped run the TOMCAT CTM

VC: helped to run instrumentation onboard the Falcon, assisted in the SHIVA campaign planning, and edited the manuscript.

AAS: helped in the interpretation of the meteorological results.

MD: helped in the planning and implementation of the SHIVA aircraft campaign

PSM: helped enable the SHIVA campaign to take place in Malaysia.

LKP: helped enable the SHIVA campaign to take place in Malaysia.

HS: helped in the planning and implementation of the SHIVA aircraft campaign

KP: headed the planning and implementation of the SHIVA aircraft campaign

Competing interests. The authors declare that they have no conflict of interest.

Acknowledgements. This work was supported by the EU Stratospheric Ozone: Halogen Impacts in a Varying Atmosphere (SHIVA) project (SHIVA-226224-FP7-ENV-2008-1). We are grateful to the support given by the National Oceanography Directorate (NOD) and the Economic Planning Unit (EPU) of Malaysia. In particular, we are grateful for the support given by Prof. Dr. Nor Aieni Binti Haji Mokhtar (NOD) and Mrs. Munirah Abd Manan (EPU) without which the SHIVA campaign in the Western Pacific would not have been possible. We would like to acknowledge the use of computing hours on the FUXI high performance computer at the Laboratoire d'Aérologie, Toulouse, France. We thank B. Quack for substantial comments and advice on the manuscript preparation. CATT-BRAMS is a free software provided by CPTEC/INPE and distributed under the CC-GNU-GPL license. RH is supported by a NERC Independent Research Fellowship (NE/N014375/1). EA was supported by funds from NASA Upper Atmosphere Program (Grant NNX17AE43G). For CJH.

References

Andrews, S. J., Carpenter, L. J., Apel, E. C., Atlas, E., Donets, V., Hopkins, J. R., Hornbrook, R. S., Lewis, A. C., Lidster, R. T., Lueb, R., Minaeian, J., Navarro, M., Punjabi, S., Riemer, D., and Schauffler, S.: A comparison of very short lived halocarbon (VSLS) and DMS aircraft measurements in the tropical west Pacific from CAST, ATTREX and CONTRAST, Atmos. Meas. Tech., 9, 5213–5225, https://doi.org/10.5194/amt-9-5213-2016, 2016.

Ashfold, M.J., Harris, N.R.P., Manning, A.J., Robinson, A.D., Warwick, N.J., and Pyle, J.A.: Estimates of tropical bromoform emissions using an inversion method, Atmos. Chem. Phys., 14 (2), 979-994, doi: 10.5194/acp-14-979-2014, 2014.

Aschmann, J., and Sinnhuber, B.-M.: Contribution of very short-lived substances to stratospheric bromine loading: Uncertainties and constraints, Atmos. Chem. Phys., 13 (3), 1203-1219, doi: 10.5194/acp-13-1203-2013, 2013.

Barth, M. C., Stuart, A. L., and Skamarock, W. C.: Numerical simulations of the July 10, 1996, Sratospheric-tropospheric experiment: radiation, aerosols and ozone (STERAO)- Deep convection experiment storm: redistribution of soluble tracers, J. Geophys. Res.,106(D12), 12,381-12,400, 2001.

https://doi.org/10.5194/acp-2020-655
Preprint. Discussion started: 1 September 2020


Atmospheric Chemistry and Physics Discussions

Barth, M. C., Kim, S.-W., Skamarock, W. C., Stuart, A. L., Pickering, K. E., and Ott, L. E.: Simulations of the redistribution of formaldehyde, fomic acid, and peroxides in the July 1996 stratospheric-tropospheric experiment: radiation, aerosols and ozone deep convection storm, J. Geophys. Res., 112, D13310, doi:10.1029/2006JD008046, 2007.

Burkholder, J.B., Hodnebrog, Ø., and Orkin, V.L.: Appendix A - Summary of Abundances, Lifetimes, Ozone Depletion Potentials (ODPs), Radiative Efficiencies (REs), Global Warming Potentials (GWPs), and Global Temperature change Potentials (GTPs), Global Ozone Research and Monitoring Project–Report No. 58, World Meteorological Organization, Geneva, Switzerland, 2018.

Butler, J.H., King, D.B., Lobert, J.M., Montzka, S.A., Yvon-Lewis, S.A., Hall, B.D., Warwick, N.J., Mondeel, D.J., Aydin, M., and Elkins, J.W.: Oceanic distributions and emissions of short-lived halocarbons, Global Biogeochem. Cycles, 21, GB1023, doi: 10.1029/2006GB002732, 2007.

Butler, R., Palmer, P. I., Feng, L., Andrews, S. J., Atlas, E. L., Carpenter, L. J., Donets, V., Harris, N. R. P., Montzka, S. A., Pan, L. L., Salawitch, R. J., and Schauffler, S. M.: Quantifying the vertical transport of $CHBr_3$ and CH_2Br_2 over the western Pacific, Atmos. Chem. Phys., 18, 13135-13153, https://doi.org/10.5194/acp-18-13135-2018, 2018.

Carpenter, L. J., Jones, C. E., Dunk, R. M., Hornsby, K. E., and Woeltjen, J.: Air-sea fluxes of biogenic bromine from the tropical and North Atlantic Ocean, Atmos. Chem. Phys., 9, 1805–1816, https://doi.org/10.5194/acp-9-1805-2009, 2009.

Carpenter, L., Reimann, S., Burkholder, J., Clerbaux, C., Hall, B., Hossaini, R., Laube, J., and Yvon-Lewis, S.: Chapter 1: Update on Ozone-Depleting Substances (ODSs) and Other Gases of Interest to the Montreal Protocol, pp. 21–125, Global Ozone Research and Monitoring Project Report, World Meteorological Organization (WMO), 2014.

Catoire V, Robert C, Chartier M, Jacquet P, Guimbaud C, Krysztofiak G: The SPIRIT airborne instrument: a three-channel infrared absorption spectrometer with quantum cascade lasers for in-situ atmospheric trace-gas measurements. Applied Physics B 123: 244. https:// doi.org/10.1007/s00340-017-6820-x, 2017.

Chipperfield, M.: New version of the TOMCAT/SLIMCAT offline chemical transport model: intercomparison of stratospheric tracer experiments, Q. J. Roy. Meteor. Soc., 132, 1179–1203, doi:10.1256/qj.05.51, 2006.

Corti, T., B. P. Luo T. Peter H. Vömel Q. Fu.: Mean radiative energy balance and vertical mass fluxes in the equatorial upper troposphere and lower stratosphere, Geophysical Research Letters, https://doi.org/10.1029/2004GL021889, 32 (6), 2005.

Corti, T., Luo, B. P., Fu, Q., Vömel, H., and Peter, T.: The impact of cirrus clouds on tropical troposphere-to-stratosphere transport, Atmos. Chem. Phys., 6, 2539-2547, https://doi.org/10.5194/acp-6-2539-2006, 2006.

Crassier, V., Suhre, K., Tulet, P. and Rosset, R.: Development of a reduced chemical scheme for use in mesoscale meteorological models, Atmospheric Environment, 34, 2633-2644, 2000.

Crumeyrolle, S., Gomes, L., Tulet, P., Matsuki, A., Schwarzenboeck, A., and Crahan, K.: Increase of the aerosol hygroscopicity by cloud processing in a mesoscale convective system: a case study from the AMMA campaign, Atmos. Chem. Phys., 8, 6907–6924, https://doi.org/10.5194/acp-8-6907-2008, 2008.

Dorf, M., J. H. Butler, A. Butz, C. Camy-Peyret, M. P. Chipperfield, L. Kritten, S. A. Montzka, B. Simmes, F. Weidner, and K. Pfeilsticker: Long-term observations of stratospheric bromine reveal slow down in growth, Geophys. Res. Lett., Vol. 33,

doi:10.1029/2006GL027714, 2006.

Engel, A. and M. Rigby (Lead Authors), J.B. Burkholder, R.P. Fernandez, L. Froidevaux, B.D. Hall, R. Hossaini, T. Saito, M.K. Vollmer, and B. Yao: Update on Ozone-Depleting Substances (ODSs) and Other Gases of Interest to the Montreal Protocol, Chapter 1 in Scientific Assessment of Ozone Depletion: 2018, Global Ozone Research and Monitoring Project–Report No. 58, World Meteorological Organization, Geneva, Switzerland, 2018

Fiehn, A., Quack, B., Hepach, H., Fuhlbrügge, S., Tegtmeier, S., Toohey, M., Atlas, E., and Krüger, K.: Delivery of halogenated very short-lived substances from the west Indian Ocean to the stratosphere during the Asian summer monsoon, Atmos. Chem. Phys., 17, 6723–6741, https://doi.org/10.5194/acp-17-6723-2017, 2017.

Fiehn, A., Quack, B., Stemmler, I., Ziska, F., and Krüger, K.: Importance of seasonally resolved oceanic emissions for bromoform delivery from the tropical Indian Ocean and west Pacific to the stratosphere, Atmos. Chem. Phys., 18, 11973–11990, https://doi.org/10.5194/acp-18-11973-2018, 2018.

Freitas, S. R., Longo, K. M., Silva Dias, M. A. F., Chatfield, R., Silva Dias, P., Artaxo, P., Andreae, M. O., Grell, G., Rodrigues, L. F., Fazenda, A., and Panetta, J.: The Coupled Aerosol and Tracer Transport model to the Brazilian developments of the Regional Atmospheric Modeling System (CATT-BRAMS). Part 1: model description and evaluation, Atmos. Chem. Phys., 9, 2843–2861, 2009.

Fuhlbrügge, S., Quack, B., Tegtmeier, S., Atlas, E., Hepach, H., Shi, Q., Raimund, S., and Krüger, K.: The contribution of oceanic halocarbons to marine and free tropospheric air over the tropical West Pacific, Atmos. Chem. Phys., 16, 7569–7585, https://doi.org/10.5194/acp-16-7569-2016, 2016.

Grell, G. A. and Dévényi, D.: A generalized approach to parameterizing convection combining ensemble and data assimilation, Geophys. Res. Lett., 29, 1693, doi:10.1029/2002GL015311, 2002.

Hamada, A., and Nishi, N.: Development of a cloud-top height estimation method by geostationary satellite split-window measurements trained with Cloud-Sat data, J. App. Meteor. Clim., 49: 2035-2049, 2010.

Hossaini, R., Chipperfield, M. P., Monge-Sanz, B. M., Richards, N. A. D., Atlas, E., and Blake, D. R.: Bromoform and dibromomethane in the tropics: a 3-D model study of chemistry and transport, Atmos. Chem. Phys., 10, 719–735, doi:10.5194/acp-10-719-2010, 2010.

Hossaini, R., Chipperfield, M. P., Feng, W., Breider, T. J., Atlas, E., Montzka, S. A., Miller, B. R., Moore, F., and Elkins, J.: The contribution of natural and anthropogenic very short-lived species to stratospheric bromine, Atmos. Chem. Phys., 12, 371–380, doi:10.5194/acp-12-371-2012, 2012.

Hossaini, R., Mantle, H., Chipperfield, M. P., Montzka, S. A., Hamer, P., Ziska, F., Quack, B., Krüger, K., Tegtmeier, S., Atlas, E., Sala, S., Engel, A., Bönisch, H., Keber, T., Oram, D., Mills, G., Ordóñez, C., Saiz-Lopez, A., Warwick, N., Liang, Q., Feng, W., Moore, F., Miller, B. R., Marécal, V., Richards, N. A. D., Dorf, M., and Pfeilsticker, K.: Evaluating global emission inventories of biogenic bromocarbons, Atmos. Chem. Phys., 13, 11819-11838, https://doi.org/10.5194/acp-13-11819-2013, 2013.

https://doi.org/10.5194/acp-2020-655
Preprint. Discussion started: 1 September 2020

Atmospheric Chemistry and Physics Discussions

Hossaini, R., Patra, P. K., Leeson, A. A., Krysztofiak, G., Abraham, N. L., Andrews, S. J., Archibald, A. T., Aschmann, J., Atlas, E. L., Belikov, D. A., Bönisch, H., Carpenter, L. J.,Dhomse, S., Dorf, M., Engel, A., Feng, W., Fuhlbrügge, S., Griffiths, P. T., Harris, N. R. P., Hommel, R., Keber, T., Krüger, K., Lennartz, S. T., Maksyutov, S., Mantle, H., Mills, G. P., Miller, B., Montzka, S. A., Moore, F., Navarro, M. A., Oram, D. E., Pfeilsticker, K., Pyle, J. A., Quack, B., Robinson, A.D., Saikawa, E., Saiz-Lopez, A., Sala, S., Sinnhuber, B.-M.,Taguchi, S., Tegtmeier, S., Lidster, R. T., Wilson, C., and Ziska, F.: A multi-model intercomparison of halogenated very short- lived substances (TransCom-VSLS): linking oceanic emissions and tropospheric transport for a reconciled estimate of the stratospheric source gas injection of bromine, Atmos. Chem. Phys., 16, 9163–9187, https://doi.org/10.5194/acp-16-9163-2016, 2016.

Hoyle, C. R., V. Marécal**,** M. R. Russo, G. Allen, J. Arteta, C. Chemel, M. P. Chipperfield, F. D'Amato, O. Dessens, W. Feng, J. F. Hamilton, N. R. Harris, J. S. Hosking, A. C. Lewis, O. Morgenstern, T. Peter, J. A. Pyle, T. Reddmann, N. A. D. Richards, P. J. Telford, W. Tian, S. Viciani, A Volz-Thomas, O. Wild, X. Yang and G. Zeng: Representation of tropical deep convection in atmospheric models. Part 2: Tracer transport. Atmos. Chem. Phys**.,** 11, 8103–8131, 2011.

Iwasaki, S., Shibata, T., Nakamoto, J., Okamoto, H., Ishimoto, H., and Kubota, H.: Characteristics of deep convection measured by using the A-Train constellation, J. Geophys. Res., 115: D06207. https://doi.org/10.1029/2009JD013000, 2010.

Johnson, R. H., and Priegnitz, D. L.: Winter monsoon convection in the vicinity of North Borneo. Part II: effects on large-scale fields, Mon. Wea. Rev., 109, 1615-1628, 1981.

Keber, T., Bönisch, H., Hartick, C., Hauck, M., Lefrancois, F., Obersteiner, F., Ringsdorf, A., Schohl, N., Schuck, T., Hossaini, R., Graf, P., Jöckel, P., and Engel, A.: Bromine from short-lived source gases in the extratropical northern hemispheric upper troposphere and lower stratosphere (UTLS), Atmos. Chem. Phys., 20, 4105–4132, https://doi.org/10.5194/acp-20-4105-2020, 2020.

Krysztofiak, G., V., Catoire, G., Poulet, V., Marécal, M., Pirre, F., Louis, S., Canneaux, and B. Josse: Detailed modeling of the atmospheric degradation mechanism of very-short lived brominated species. Atmos. Env., 59, 514-532, 2012.

Krysztofiak, G., V. Catoire, P. D. Hamer, V. Marécal, C. Robert, A. Engel, H. Bönisch, K. Grossman, B. Quack, E. Atlas and K. Pfeilsticker: Evidence of convective transport in tropical West Pacific region during SHIVA experiment, DOI :10/1002/asl.798, Atmos. Sci. Letters, 2018.

Leedham, E. C., Hughes, C., Keng, F. S. L., Phang, S.-M., Malin, G., and Sturges, W. T.: Emission of atmospherically significant halocarbons by naturally occurring and farmed tropical macroalgae, Biogeosciences, 10, 3615–3633, https://doi.org/10.5194/bg-10-3615-2013, 2013.

Liang, Q., Stolarski, R. S., Kawa, S. R., Nielsen, J. E., Douglass, A. R., Rodriguez, J. M., Blake, D. R., Atlas, E. L., and Ott, L. E.: Finding the missing stratospheric Br_y: a global modeling study of $CHBr_3$ and CH_2Br_2 , Atmos. Chem. Phys., 10, 2269–2286, doi:10.5194/acp-10-2269-2010, 2010.

Liang, Q., E. Atlas, D. Blake, M. Dorf, K. Pfeilsticker, and S. Schauffler: Convective transport of very-short-lived bromocarbons to the stratosphere, Atmos. Chem. Phys., 14, 5781-5792, doi: 10.5194/acp-14-5781 2014, 2014.

Liu, C. and Zisper, E.J.: Global distribution of convection penetrating the tropical tropopause: Journal of Geophysical Research:

785 Atmospheres, 110 (D23), 16, 2005.

Longo, K. M., S. R. Freitas, M. Pirre, V. Marécal, L. F. Rodrigues, J. Panetta, M. F. Alonso, N. E. Rosário, D. S. Moreira, M. S. Gácita, J. Arteta, R. Fonseca, R. Stockler, D. M. Katsurayama, A. Fazenda, M. Bela: The Chemistry CATT-BRAMS model (CCATT-BRAMS 4.5): a regional atmospheric model system for integrated air quality and weather forecasting and research, Geosci. Mod. Dev., 6, 1389-1405, 2013.

790 Luo, Z., G. Y. Liu, and G. L. Stephens, CloudSat adding new insight into tropical penetrating convection, Geophys. Res. Lett., 35, L19819, doi:10.1029/2008GL035330, 2008.

McLinden, C. A., Haley, C. S., Lloyd, N. D., Hendrick, F., Rozanov, A., Sinnhuber, B.-M., Goutail, F., Degenstein, D. A., Llewellyn, E. J., Sioris, C. E., Van Rozendael, M., Pommereau, J. P., Lotz, W., and Burrows, J. P.: Odin/OSIRIS observations of stratospheric BrO: Retrieval methodology, climatology, and inferred Br_y , J. Geophys. Res.-Atmos., 115, D15308,

795 doi:10.1029/2009JD012488, 2010.

Marécal V., E. Rivière, G. Held, S. Cautenet and S. Freitas: Modelling study of the impact of deep convection on the UTLS air composition. Part I: analysis of ozone precursors. Atmos. Chem. Phys., 6, 1567-1584, 2006.

Marécal, M., Pirre, M., Krysztofiak, G., Hamer, P. D., and Josse, B.: What do we learn about bromoform transport and chemistry in deep convection from fine scale modelling? Atmos. Chem. Phys., 12, 6073–6093, 2012.

800 McConnell, J. C., Henderson, G. S., Barrie, L., Bottenheim, J., Niki, H., Langford, C. H., & Templeton, E. M. J: Photochemical bromine production implicated in Arctic boundary-layer ozone depletion: Nature, 355(6356), 150-152, 1992.

Mellor, G. and Yamada, T.: Development of a turbulence closure model for geophysical fluid problems, Rev. Geophys., 20, 851–875, 1982.

Meylan,W.M., Howard, P.H.: Bond contribution method for estimating Henry'slaw constants. Environmental Toxicology and

805 Chemistry 10, 1283e1293, 1991.

Montzka, S. A. and Reimann, S.: Ozone-depleting substances (ODSs) and related chemicals, in: Scientific Assessment of Ozone Depletion: 2010, Global Ozone Research and Monitoring Project, Report No. 52, Chapt. 1, edited by: World Meteorological Organization, Geneva, Switzerland, 2011.

Navarro, M. A., Atlas, E. L., Saiz-Lopez, A., Rodriguez-Lloveras, X., Kinnison, D. E., Lamarque, J. F., Tilmes, S., Filus, M.,

810 Harris, N. R. P., Meneguz, E., Ashfold, M. J.: Airborne measurements of organic bromine compounds in the Pacific tropical tropopause layer. Proceedings of the National Academy of Sciences, 112(45), 13789-13793, 2015.

Nirmalakhandan, N.N., Speece, R.E.: Prediction of aqueous solubility of organic chemicals based on molecular Structure. Environmental Science and Technology 22, 328e338, 1988.

Oppenheimer, C., Tsanev, V.I., Braban, C.F., Cox, R.A., Adams, J.W., Aiuppa, A., Bobrowski, N., Delmelle, P., Barclay, J.

815 and McGonigle, A.J.: BrO formation in volcanic plumes: Geochimica et Cosmochimica Acta, 70(12), 2935-2941, 2006.

Ordoñez, C., J.-F. Lamarque, S. Tilmes, D. E. Kinnison, E. L. Atlas, D. R. Blake, G. Sousa Santos, G. Brasseur, and A. Saiz-Lopez: Bromine and iodine chemistry in a global chemistry-climate model: description and evaluation of very short-lived oceanic sources, Atmos. Chem. Phys., 12, 1423–1447, 2012.

Pfeilsticker, K., Dorf, M., Sturges, B., Oram, D., Engel, A., Rex, M., Bracher, A., Van Roozendael, M., Hendrick, F., Theys, N., Kruger, K., Quack, B., Wallace, D., Fueglistaler, S., Pyle, J., Marecal, V., Catoire, V., Pirre, M., Chipperfield, M., Heard, D., Stohl, A., Eckhardt, S., Sinnhuber, B.-M., Rozanov, A., Wittrock, F., Schlager, H., Samah, A.A., Phang, S.M., Anton, A., Sentian, J., Lim, P.T., Mujahid, A., Abdullah, N.A., Maznorizan, Mokhtar, N.A.B.H.: The SHIVA Western Pacific campaign in fall 2011, Malaysian Journal of Science, Vol. 32, Issue Spec.Iss., 141-148, 2013.

Pyle, J. A., Ashfold, M. J., Harris, N. R. P., Robinson, A. D., Warwick, N. J., Carver, G. D., Gostlow, B., O'Brien, L. M., Manning, A. J., Phang, S. M., Yong, S. E., Leong, K. P., Ung, E. H., and Ong, S.: Bromoform in the tropical boundary layer of the Maritime Continent during OP3, Atmos. Chem. Phys., 11, 529–542, doi:10.5194/acp-11-529-2011, 2011.

Quack, B. and Wallace, D. W. R.: Air-sea flux of bromoform: Controls, rates, and implications, Global Biogeochem. Cy., 17, 1023,https://doi.org/10.1029/2002GB001890, 2003.

Rex, M., Wohltmann, I., Ridder, T., Lehmann, R., Rosenlof, K., Wennberg, P., Weisenstein, D., Notholt, J., Krüger, K., Mohr, V., and Tegtmeier, S.: A tropical West Pacific OH minimum and implications for stratospheric composition, Atmos. Chem. Phys., 14, 4827-4841, https://doi.org/10.5194/acp-14-4827-2014, 2014.

Sala, S., Bönisch, H., Keber, T., Oram, D. E., Mills, G., and Engel, A.: Deriving an atmospheric budget of total organic bromine using airborne in situ measurements from the western Pacific area during SHIVA, Atmos. Chem. Phys., 14, 6903-6923, https://doi.org/10.5194/acp-14-6903-2014, 2014.

Salawitch, R.J., D.K. Weisenstein, L.J. Kovalenko, C.E. Sioris, P.O. Wennberg, K. Chance, M.K.W. Ko, and C.A. McLinden: Sensitivity of ozone to bromine in the lower stratosphere, Geophys. Res. Lett., 32, L05811, doi: 10.1029/2004GL021504, 2005.

Salawitch, R.J., T. Canty, T. Kurosu, K. Chance, Q. Liang, A. da Silva, S. Pawson, J.E. Nielsen, J.M. Rodriguez, P.K. Bhartia, X. Liu, L.G. Huey, J. Liao, R.E. Stickel, D.J. Tanner, J.E. Dibb, W.R. Simpson, D. Donohoue, A. Weinheimer, F. Flocke, D. Knapp, D. Montzka, J.A. Neuman, J.B. Nowak, T.B. Ryerson, S. Oltmans, D.R. Blake, E.L. Atlas, D.E. Kinnison, S. Tilmes, L.L. Pan, F. Hendrick, M. Van Roozendael, K. Kreher, P.V. Johnston, R.S. Gao, B. Johnson, T.P. Bui, G. Chen, R.B. Pierce, J.H. Crawford, and D.J. Jacob: A new interpretation of total column BrO during Arctic spring, Geophys. Res. Lett., 37 (21), L21805, doi:10.1029/2010GL043798, 2010.

Sioris, C. E., Kovalenko, L. J., McLinden, C. A., Salawitch, R. J., Van Roozendael, M., Goutail, F., Dorf, M., Pfeilsticker, K., Chance, K., von Savigny, C., Liu, X., Kurosu, T. P., Pommereau, J.-P., Boesch, H., and Frerick, J.: Latitudinal and vertical distribution of bromine monoxide in the lower stratosphere from Scanning Imaging Absorption Spectrometer for Atmospheric Chartography limb scattering measurements, J. Geophys. Res. Atmos., 111, D14301, doi:10.1029/2005JD006479, 2006.

Sinnhuber, B.-M., Rozanov, A., Sheode, N., Afe, O. T., Richter, A., Sinnhuber, M., Wittrock, F., Burrows, J. P., Stiller, G. P., von Clarmann, T., and Linden, A.: Global observations of stratospheric bromine monoxide from SCIAMACHY, Geophys. Res. Lett., 32, L20810,doi:10.1029/2005GL023839, 2005.

Stockwell, W. R., Kirchner, F., Kuhn, M., and Seefeld, S.: A New Mechanism for Regional Atmospheric Chemistry Modeling, J. Geophys. Res., 102, 25847–25879, 1997.

Tegtmeier, S., Atlas, E., Quack, B., Ziska, F., and Krüger, K.: Variability and past long-term changes of brominated very short-

lived substances at the tropical tropopause, Atmos. Chem. Phys., 20, 7103–7123, https://doi.org/10.5194/acp-20-7103-2020, 2020.

Tie, X., Madronich, S., Walters, S., Zhang, R., Rasch, P., and Collins, W.: Effects of clouds on photolysis and oxidants in the troposphere, J. Geophys. Res., 108, 4642, doi:10.1029/2003JD003659, 2003.

Toon, O. B., McKay, C. P., Ackerman, T. P., and Santhanan, K. L.: Rapid calculation of radiative heating rates and photodissociation rates in inhomogeneous multiple scattering atmospheres, J. Geophys. Res., 94, 16287–16301, 1989.

Tripoli, G. and Cotton, W.: The Colorado State University threedimensional cloud-mesoscale model. Part I: General theoretical framework and sensitivity experiments, J. Res. Atmos., 16, 185–219, 1982.

Tulet, P., Suhre, K., Mari, C., Solmon, F., Rosset, R.: Mixing of boundary layer and upper tropospheric ozone during a deep convective event over Western Europe. Atmospheric Environment, 36(28), 4491-4501, 2002.

Varble A., Zipser, E. J., Fridlind, A. M., Ackerman, A. S., Chaboureau, J.-P., Collis, S., Fan,, J., and Shipway, B.: Evaluation of cloud-resolving and limited area model intercomparison simulations using TWP-ICE observations: 1. Deep convective updraft properties, J. Geophys. Res., 119, 13,891-13,918, doi:10.1002/2013/2013JD21372, 2014.

Wales, P. A., Salawitch, R. J., Nicely, J. M., Anderson, D. C., Canty, T. P., Baidar, S., et al.. Stratospheric injection of brominated very short-lived substances: Aircraft observations in the Western Pacific and representation in global models. J. Geophys. Res., 123, 5690–5719. https://doi.org/10.1029/2017JD027978, 2018.

Walko, R. L., Cotton, W. R., Meyers, M. P., and Harrington, J. Y.: New RAMS cloud microphysics parameterization, Part I: the single-moment scheme, Atmos. Res., 38, 29–62, 1995.

Walko, R., Band, L., Baron, J., Kittel, F., Lammers, R., Lee, T., Ojima, D., Pielke, R., Taylor, C., Tague, C., Tremback, C., and Vidale, P.: Coupled atmosphere-biophysics-hydrology models for environmental modeling, J. Appl. Meteorol., 39, 931–944, 2000.

Warwick, N. J., Pyle, J. A., Carver, G. D., Yang, X., Savage, N. H., O'Connor, F. M., and Cox, R. A.: Global modeling of biogenic bromocarbons, J. Geophys. Res., 111, doi:10.1029/2006JD007264, 2006.

Wennberg, P.: Bromine explosion: Nature, 397(6717), 299-301, 1999.

Ziska, F., Quack, B., Abrahamsson, K., Archer, S. D., Atlas, E., Bell, T., Butler, J. H., Carpenter, L. J., Jones, C. E., Harris, N. R. P., Hepach, H., Heumann, K. G., Hughes, C., Kuss, J., Krüger, K., Liss, P., Moore, R. M., Orlikowska, A., Raimund, S., Reeves, C. E., Reifenhäuser, W., Robinson, A. D., Schall, C., Tanhua, T., Tegtmeier, S., Turner, S., Wang, L., Wallace, D., Williams, J., Yamamoto, H., Yvon-Lewis, S., and Yokouchi, Y.: Global sea-to-air flux climatology for bromoform, dibromomethane and methyl iodide, Atmos. Chem. Phys., 13, 8915–8934, doi:10.5194/acp13-8915-2013, 2013.

https://doi.org/10.5194/acp-2020-655
Preprint. Discussion started: 1 September 2020

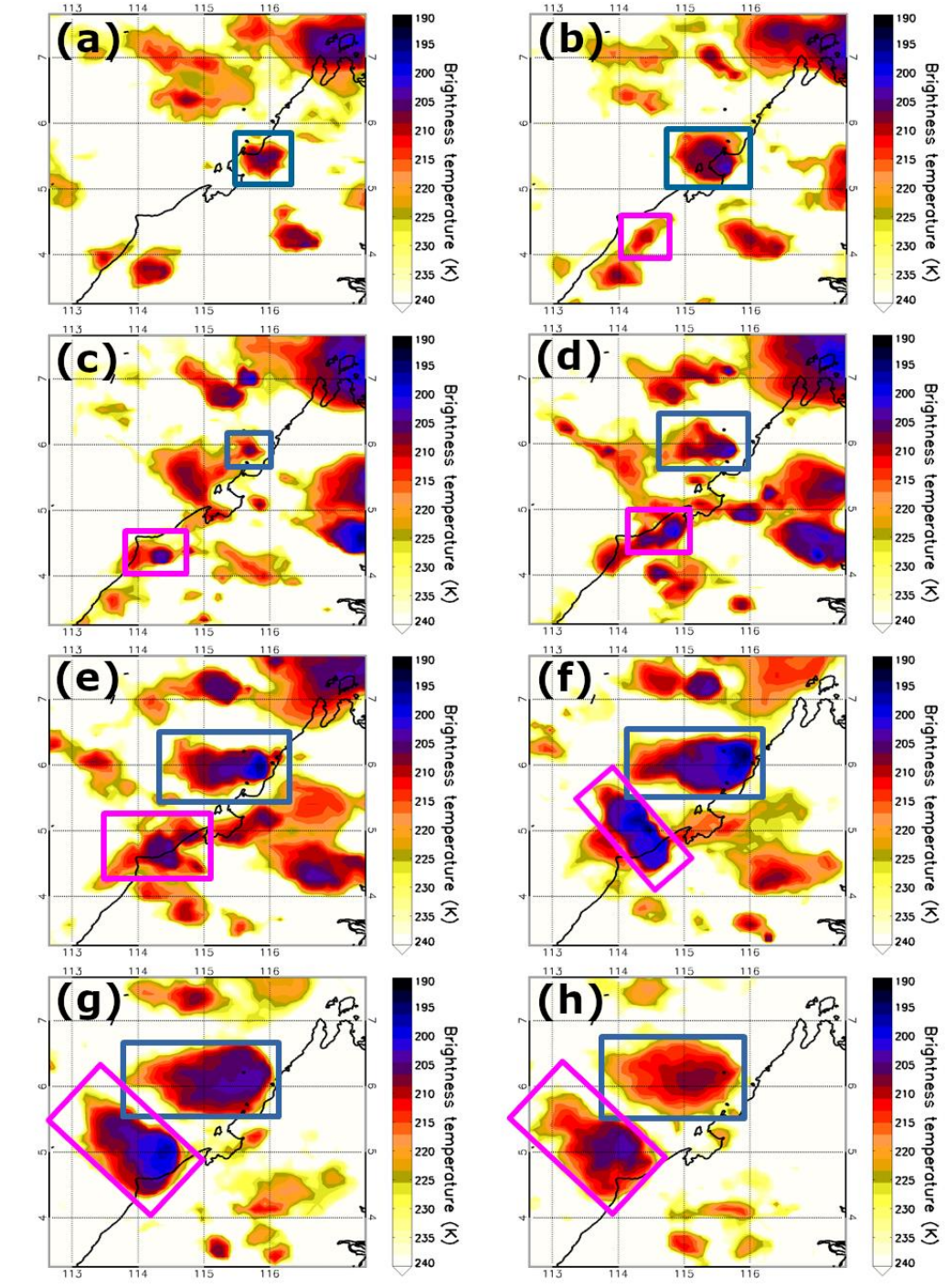

Figure 1: The contours show the brightness temperatures from MTSAT-2 at (a) 5UTC, (b) 6UTC, (c) 7UTC, (d) 8 UTC, (e) 9UTC, (f) 10 UTC, (g) 11 UTC and (h) 12UTC on November 19 2011. The system called Obs_Conv1 is shown by a blue rectangle and Obs_Conv2 by a pink rectangle. The black line shows the coast with the land to the east.

https://doi.org/10.5194/acp-2020-655
Preprint. Discussion started: 1 September 2020

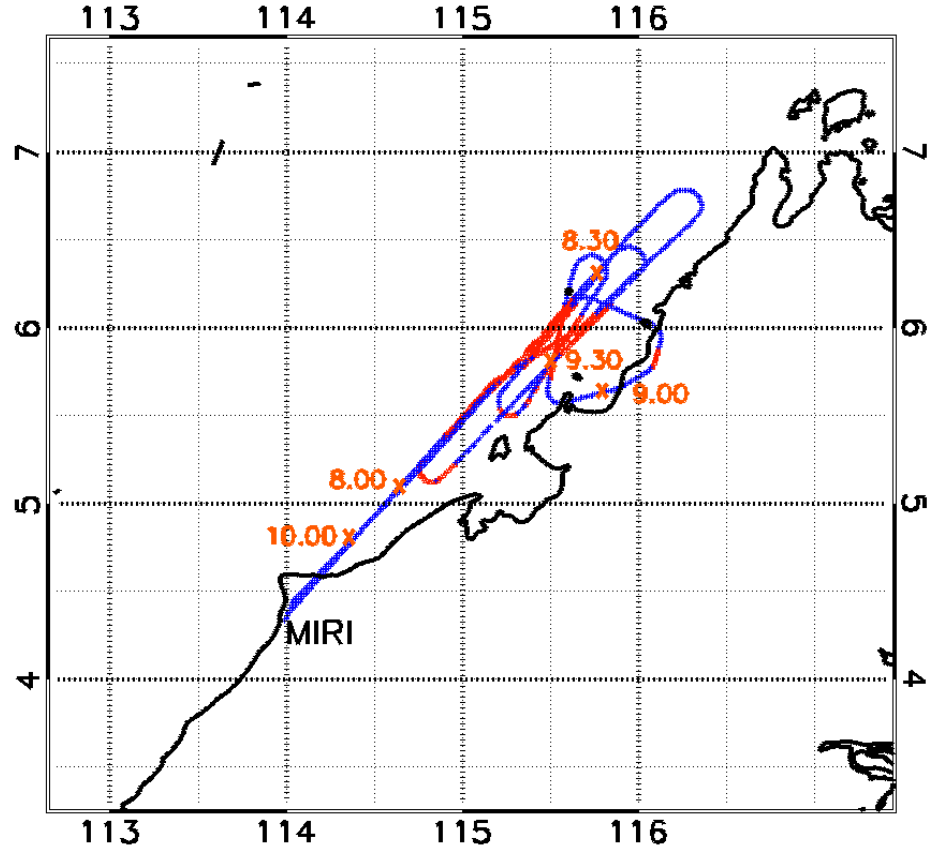

885

Figure 2: Overview of the Falcon aircraft trajectory on the afternoon of November 19, 2011. The red crosses indicate the location where the aircraft crossed convective outflows as determined in Krysztofiak et al. (2018).

https://doi.org/10.5194/acp-2020-655
Preprint. Discussion started: 1 September 2020

Atmospheric Chemistry and Physics Discussions

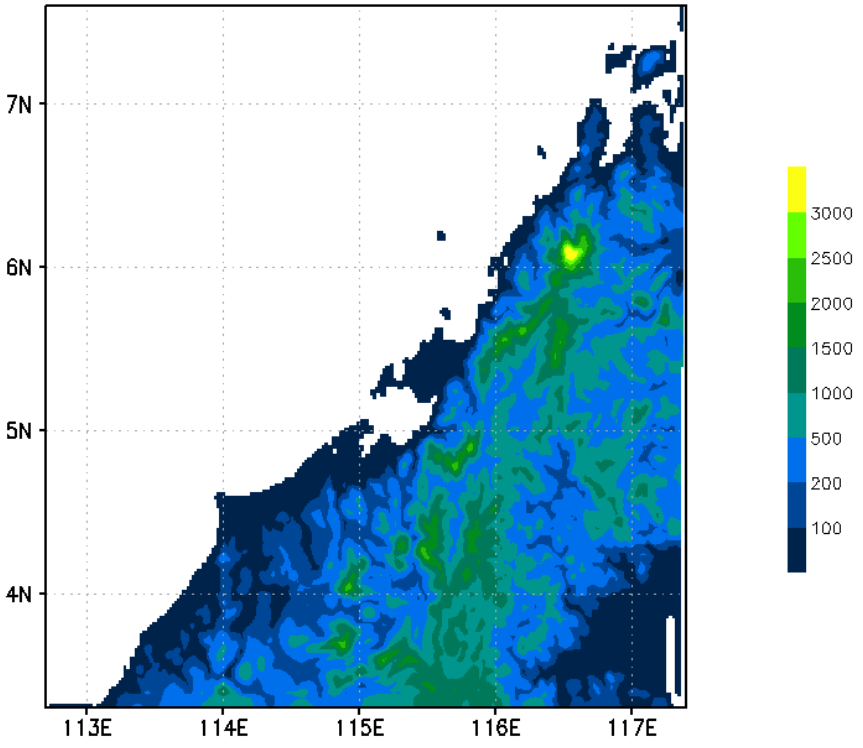

Figure 3: Map of topography used in CCATT-BRAMS for the finest scale model grid.

https://doi.org/10.5194/acp-2020-655
Preprint. Discussion started: 1 September 2020

Atmospheric Chemistry and Physics Discussions

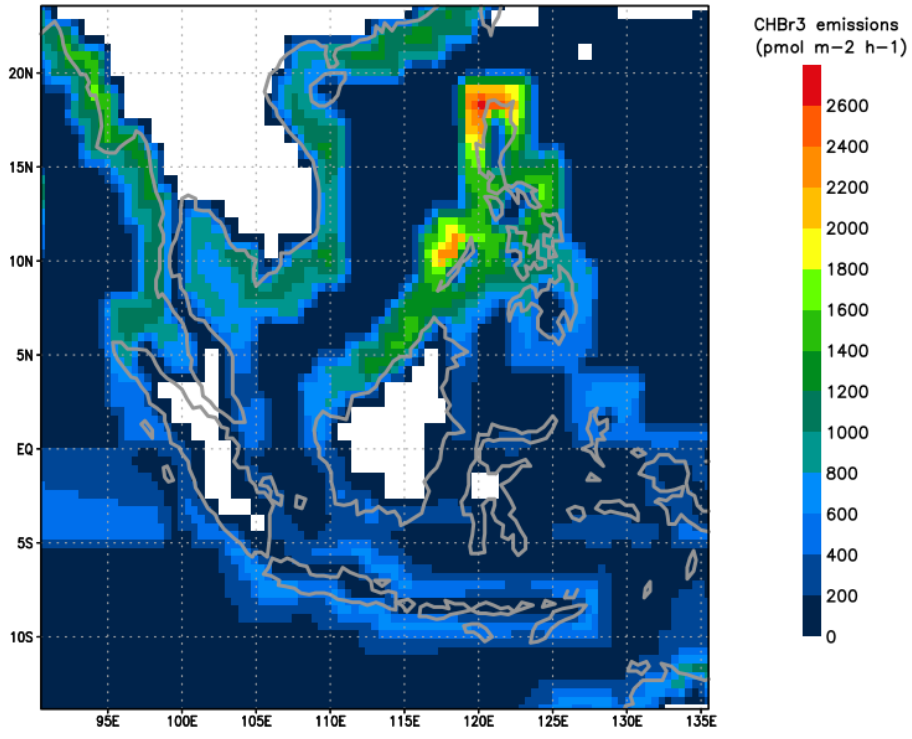

890

Figure 4: Map of the annual $CHBr_3$ emission distribution in Gg yr^{-1} used in C-CATT-BRAMS in the largest model domain (Ziska et al., 2013).

https://doi.org/10.5194/acp-2020-655
Preprint. Discussion started: 1 September 2020

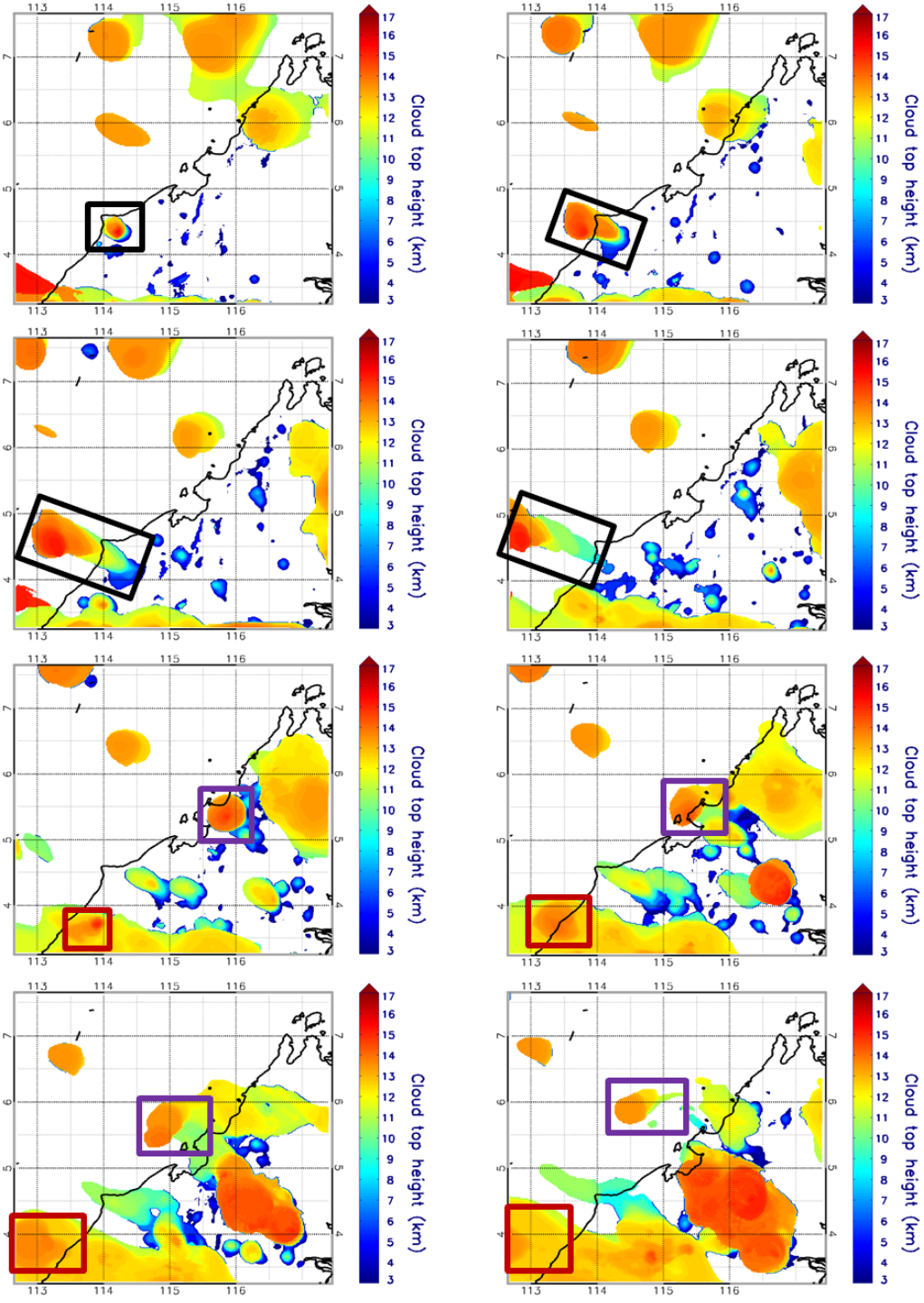

Figure 5: Simulated cloud top heights derived from the C-CATT-BRAMS model runs at the same times as the MTSAT-2 satellite observations shown in Fig. 1 (at (a) 5UTC, (b) 6UTC, (c) 7UTC, (d) 8 UTC, (e) 9UTC, (f) 10 UTC, (g) 11 UTC and (h) 12 UTC). The system called Mod_Conv1 is shown by a black rectangle Mod_Conv2 by a red rectangle, and Mod_Conv3 by a purple rectangle.

https://doi.org/10.5194/acp-2020-655
Preprint. Discussion started: 1 September 2020

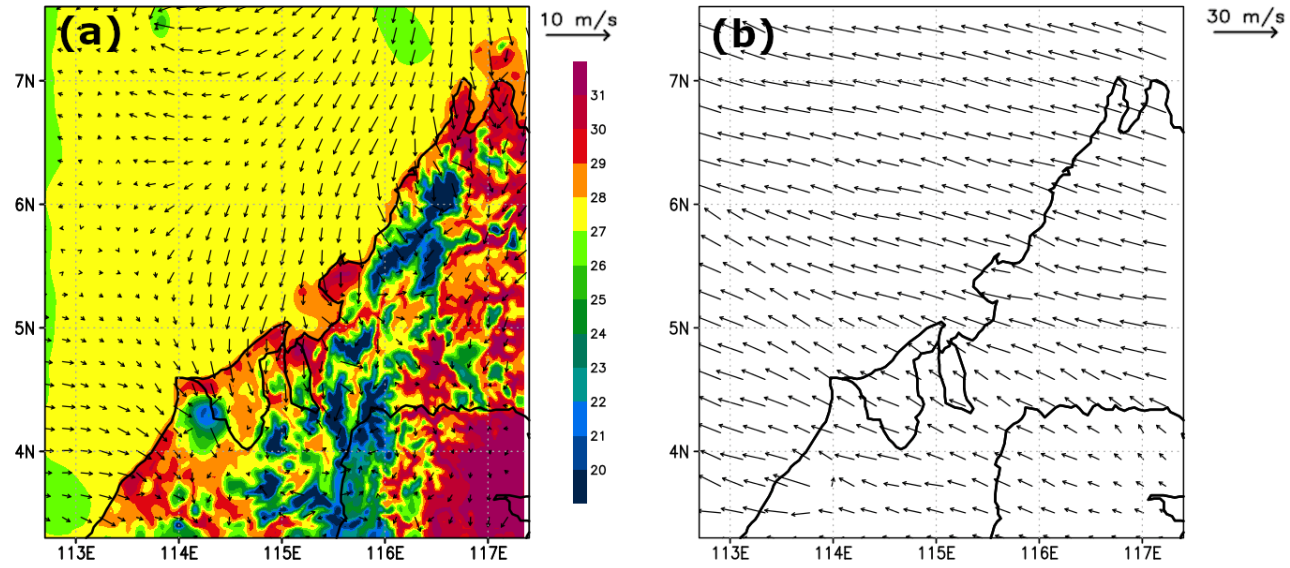

Figure 6: Simulated (a) temperature and horizontal wind at the lowest model level (24 m) at 6 UTC. (b) horizontal wind at 11700 m altitude at 9UTC from the C-CATT-BRAMS model.

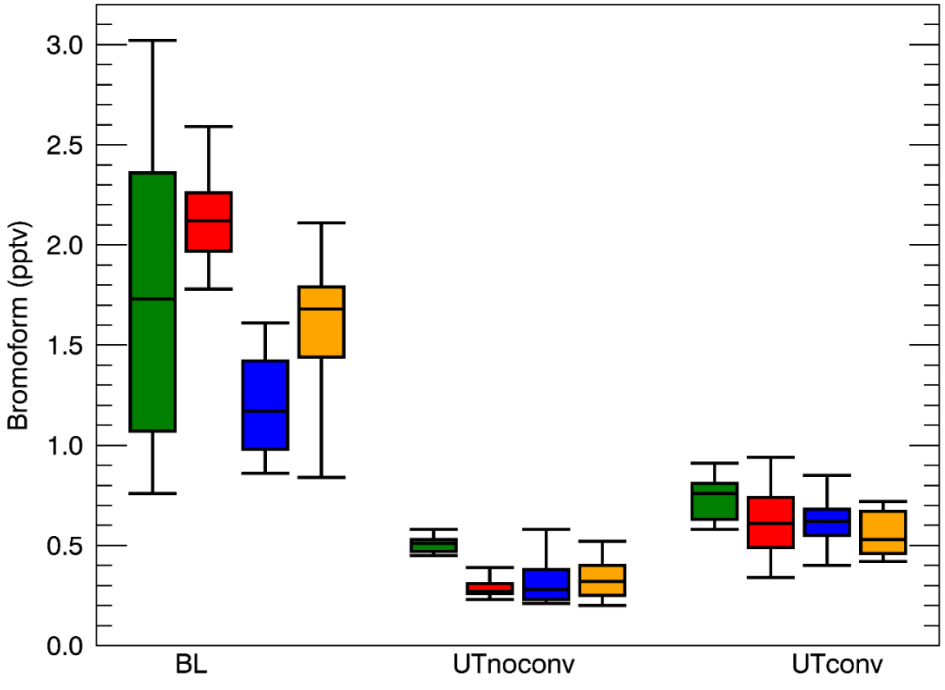

Figure 7: Box and whiskers plots (5th, 25th percentile, median, 75th percentile, 95th) for the 3 simulated convective system and from the observations of $CHBr_3$ concentrations in pptv. The green bars show the observed mixing ratios, the red, those of Mod_Conv1, the blue those of Mod_Conv2, and the orange those of Mod_Conv3. From left to right the results as shown for the boundary layer, non-convective upper troposphere and convective troposphere.

https://doi.org/10.5194/acp-2020-655
Preprint. Discussion started: 1 September 2020

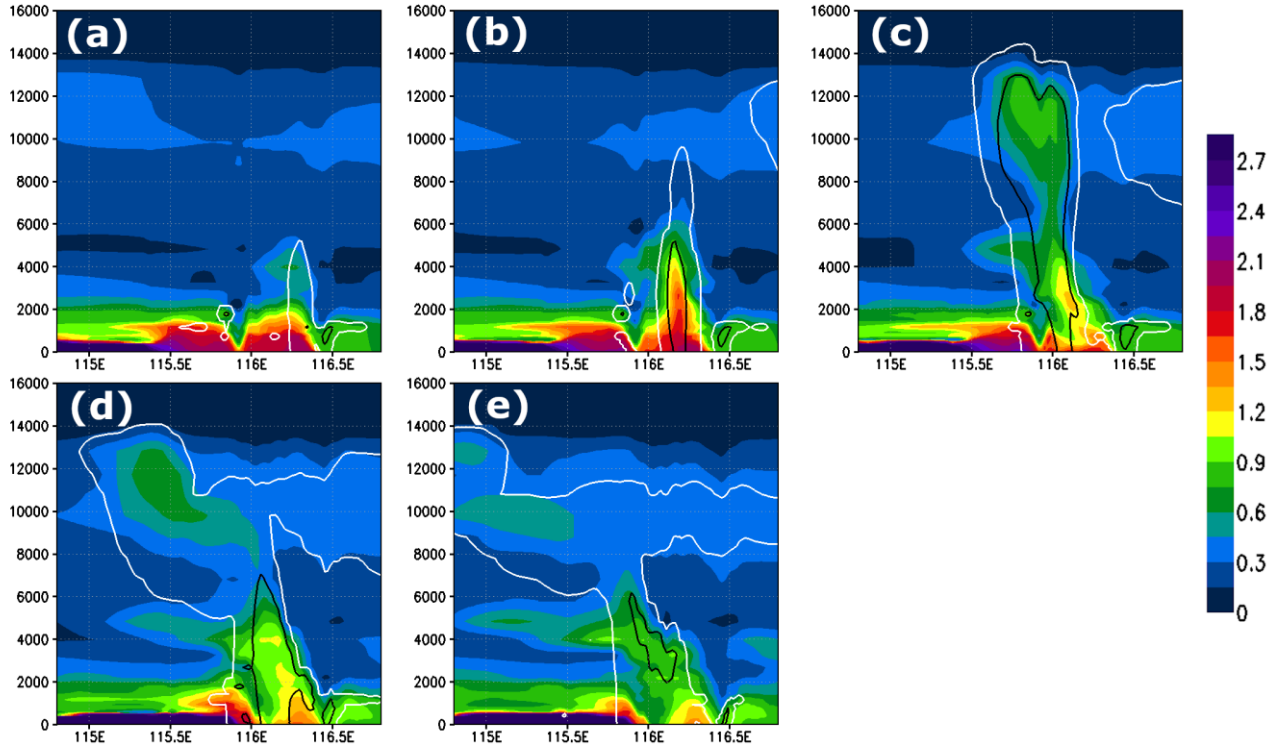

Figure 8: Vertical cross section within the most active part of Mod_Conv3 convective system showing time evolution of $CHBr_3$ mixing ratio in pptv for 7 UTC, 8 UTC, 9 UTC, 10 UTC, and 11 UTC. The white and black lines represent the 0.01g kg^{-1} and 0.5 g kg^{-1} contour of the simulated condensed water (cloud and precipitation in ice and liquid phase).

895

https://doi.org/10.5194/acp-2020-655
Preprint. Discussion started: 1 September 2020

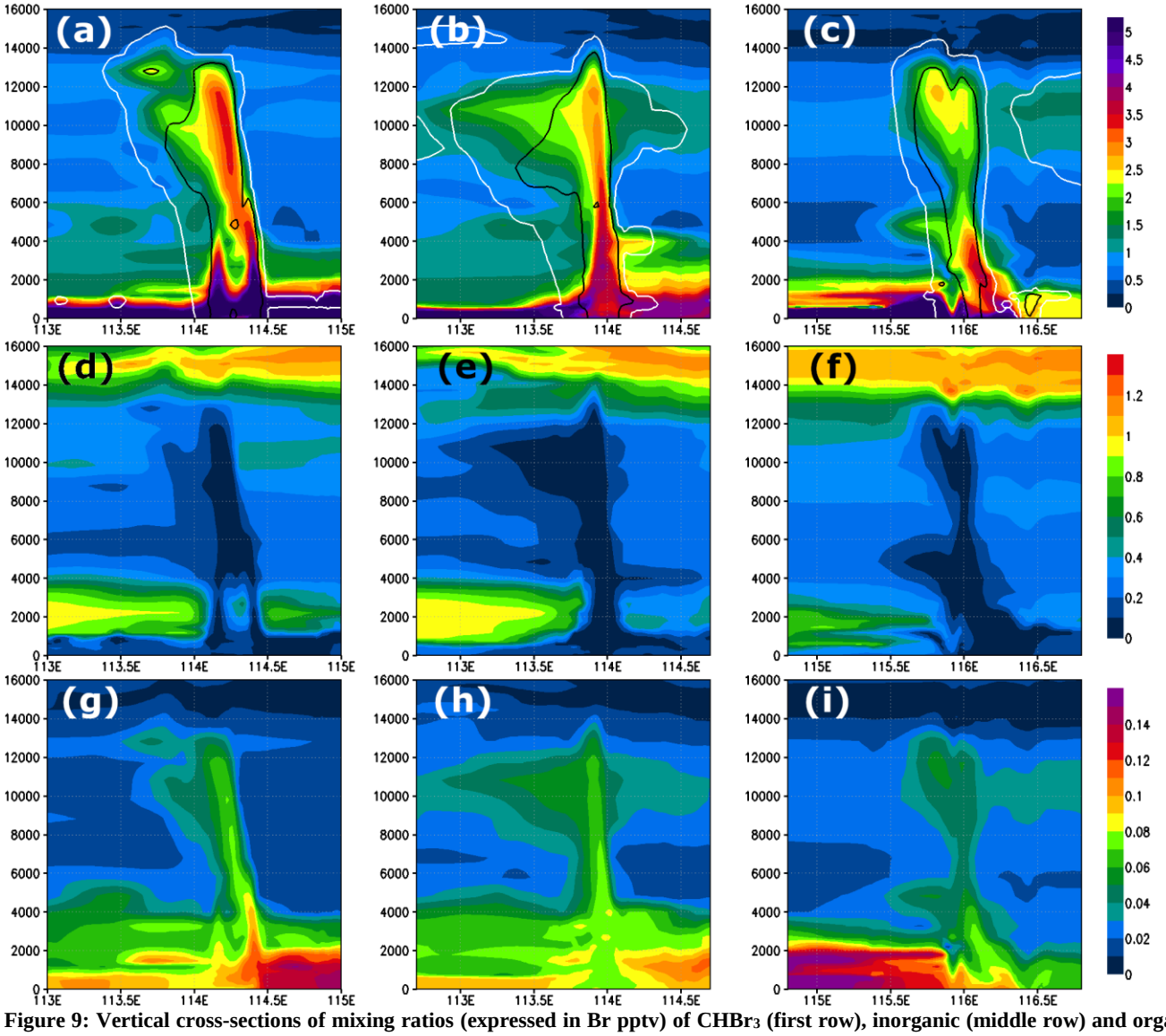

Figure 9: Vertical cross-sections of mixing ratios (expressed in Br pptv) of $CHBr_3$ (first row), inorganic (middle row) and organic (bottom row) bromine compounds. The left, middle and right columns correspond to cross sections of Mod_Conv1 at 4.35°N at 6 UTC, Mod_Conv2 at 3.75°N at 9 UTC and Mod_Conv3 at 5.4°N at 9 UTC. The white and black lines represent the 0.01g kg^{-1} and 0.5 g kg^{-1} contour of the simulated condensed water (cloud and precipitation in ice and liquid phase), respectively.

https://doi.org/10.5194/acp-2020-655
Preprint. Discussion started: 1 September 2020

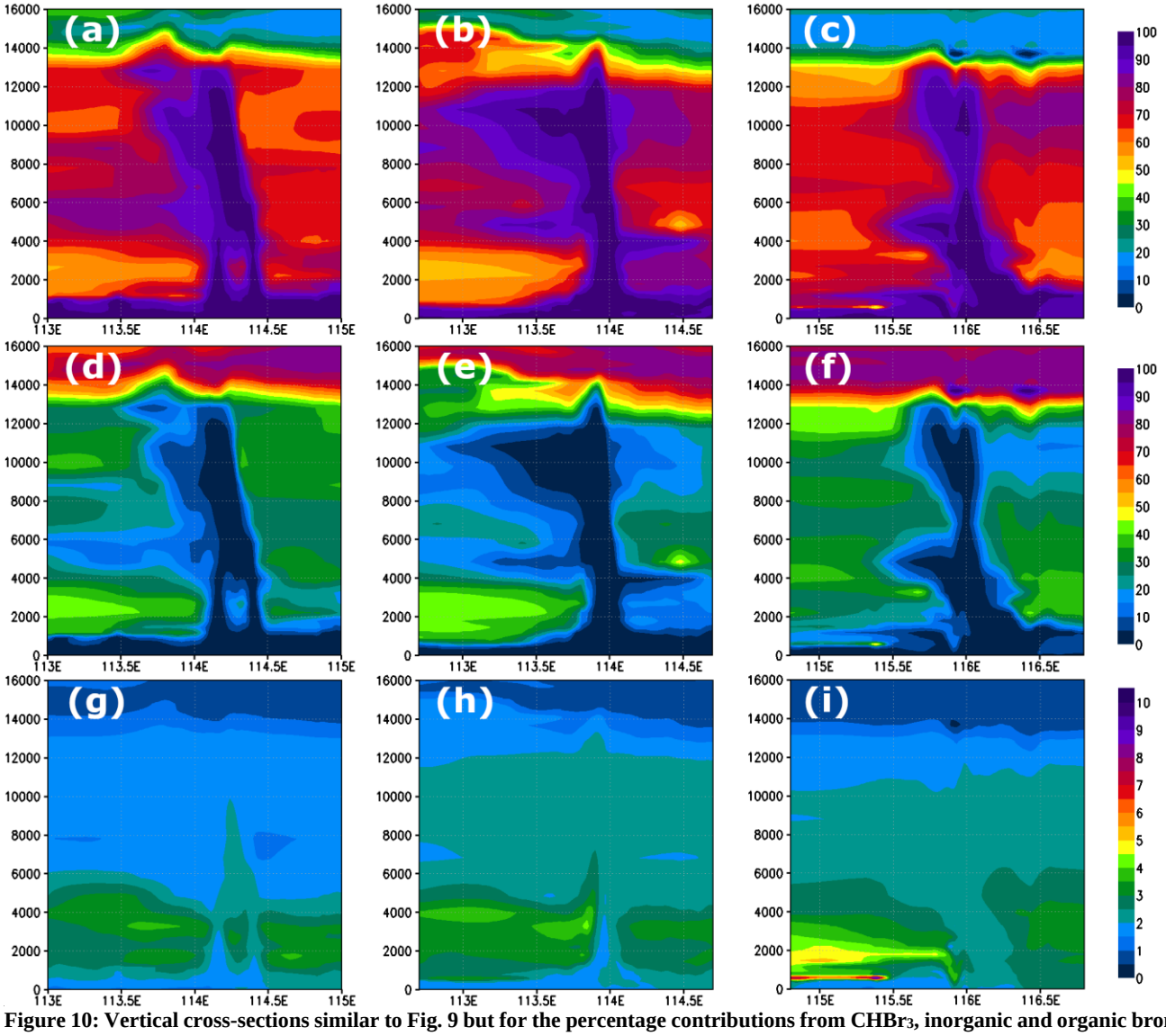

Figure 10: Vertical cross-sections similar to Fig. 9 but for the percentage contributions from $CHBr_3$, inorganic and organic bromine compounds to the total Br mixing ratio. Note that for organic bromine the scale is from 0 to 10%.

https://doi.org/10.5194/acp-2020-655
Preprint. Discussion started: 1 September 2020

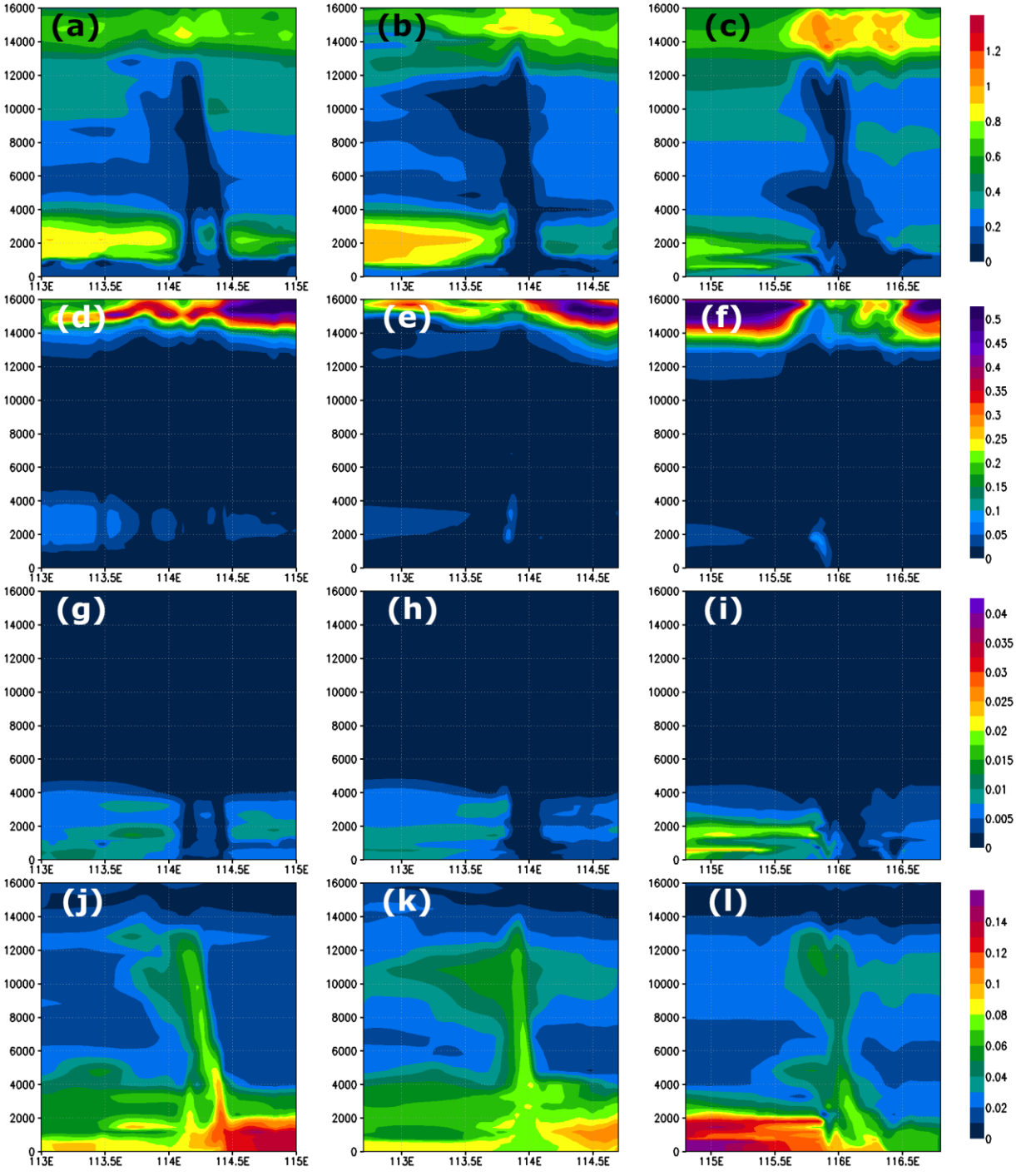

Figure 11: Vertical cross-sections of mixing ratios (expressed in Br pptv) of soluble inorganic [HOBr, HBr, and $BrONO_2$] (first row), insoluble inorganic [Br, Br_2, and BrO] (second row), soluble organic [bromo-methyl peroxides] (third row) and insoluble organic [bromo-carbonyls] (bottom row) bromine compounds. The left, middle and right columns correspond to cross sections of Mod_Conv1 at 4.35°N at 6 UTC, Mod_Conv2 at 3.75°N at 9 UTC and Mod_Conv3 at 5.4°N at 9 UTC.

https://doi.org/10.5194/acp-2020-655
Preprint. Discussion started: 1 September 2020

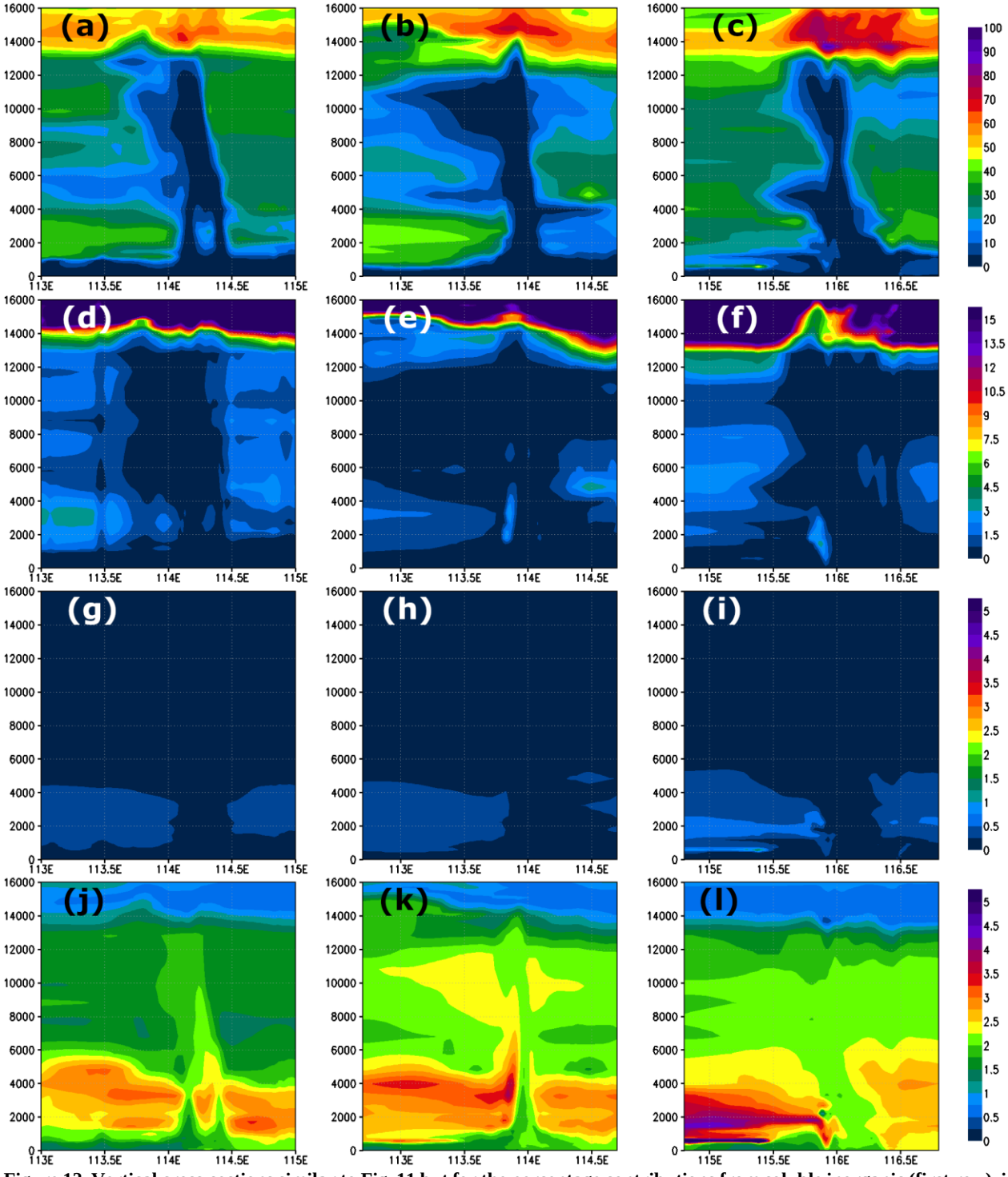

Figure 12. Vertical cross-sections similar to Fig. 11 but for the percentage contributions from soluble inorganic (first row), insoluble inorganic (second row), soluble organic (third row) and insoluble organic (bottom row) bromine compounds to the total Br mixing ratio. Note that for insoluble inorganic and organic bromine, the scale is from 0 to 5%.

https://doi.org/10.5194/acp-2020-655
Preprint. Discussion started: 1 September 2020

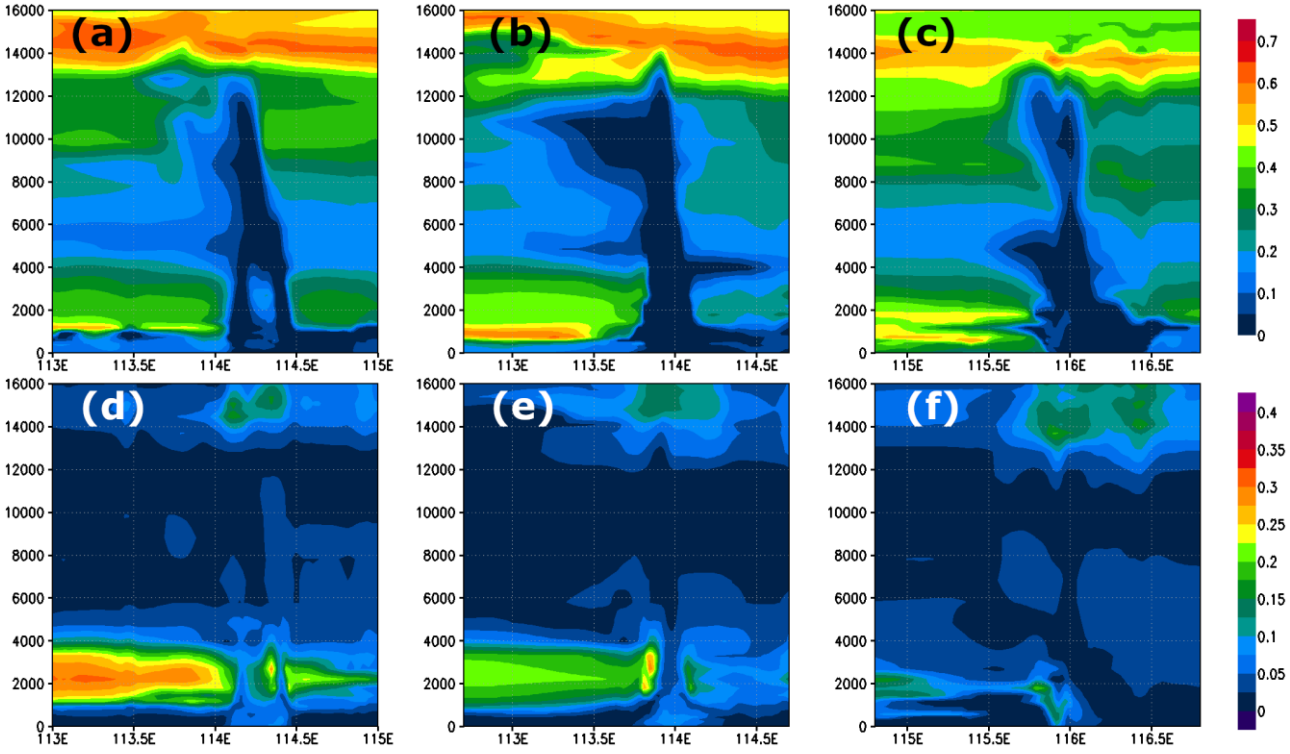

Figure 13: Vertical cross-sections of mixing ratios (expressed in Br pptv) of HBr (top row) and HOBr (bottom row) bromine compounds. The left, middle and right columns correspond to cross sections of Mod_Conv1 at 4.35°N at 6 UTC, Mod_Conv2 at 3.75°N at 9 UTC and Mod_Conv3 at 5.4°N at 9 UTC.

https://doi.org/10.5194/acp-2020-655
Preprint. Discussion started: 1 September 2020

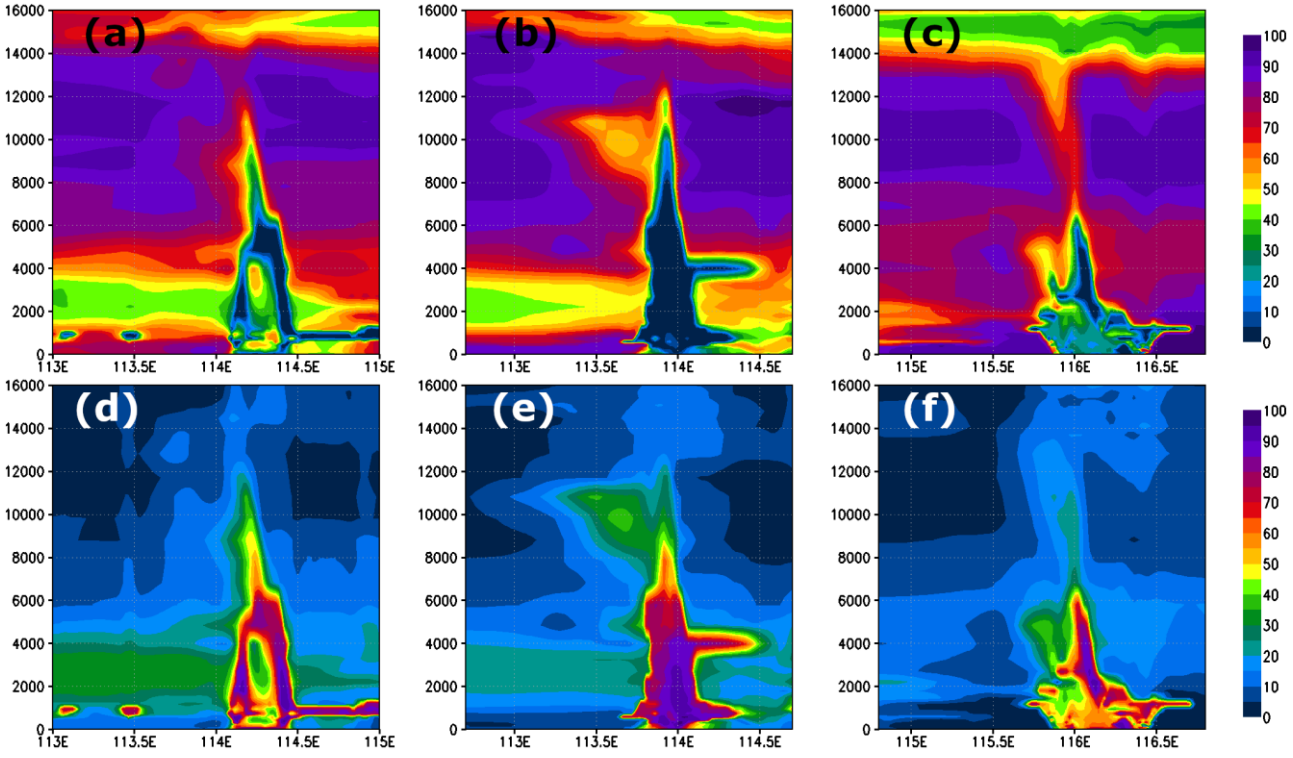

Figure 14: Vertical cross-sections similar to Fig. 13 but for the percentage contributions of HBr (top row) and HOBr (bottom row) to the total inorganic Br mixing ratio.

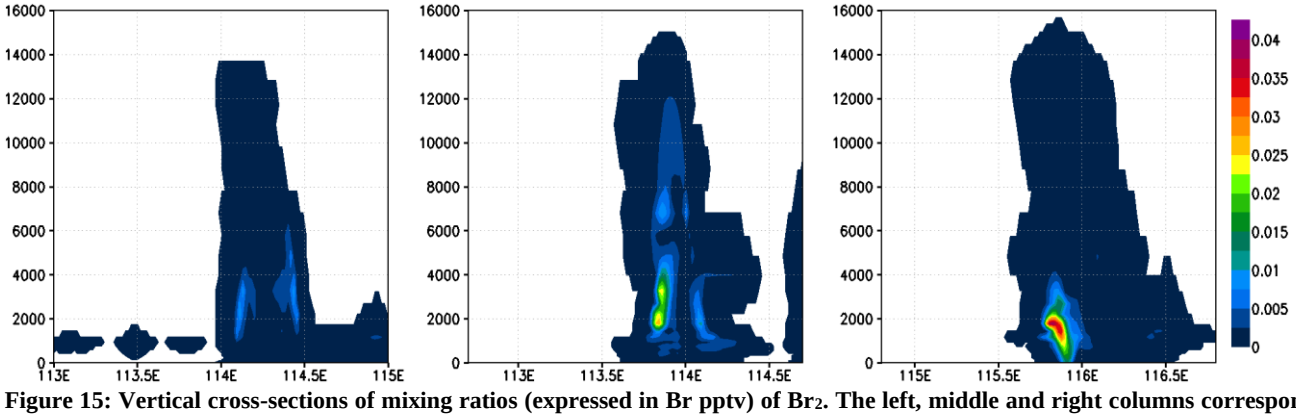

Figure 15: Vertical cross-sections of mixing ratios (expressed in Br pptv) of Br_2. The left, middle and right columns correspond to cross sections of Mod_Conv1 at 4.35°N at 6 UTC, Mod_Conv2 at 3.75°N at 9 UTC and Mod_Conv3 at 5.4°N at 9 UTC.